An EpCAM/Trop2 mechanostat differentially regulates individual and collective migration of human carcinoma cells

Azam Aslemarz[1,2], Marie-Fagotto Kaufmann[1,4], Artur Ruppel[3,5], Martial Balland[3], Paul Lasko[2] and François Fagotto[1]

[1]CRBM, University of Montpellier and CNRS, Montpellier 34293, France

[2]Dept. of Biology, McGill University, Montreal, QC, Canada H3A1B1.

[3]LIPHY, UMR5588, University of Grenoble, 38400 Grenoble, France

[4]current address: Department of Neurobiology, University of Stuttgart, 70569 Stuttgart, Germany

[5]current address: CRBM, University of Montpellier and CNRS, Montpellier 34293

Correspondence to François Fagotto, email: francois.fagotto@crbm.cnrs.fr

Abstract

EpCAM is well known as a carcinoma associated cell surface protein that is widely used as an epithelial cancer biomarker. Despite its clear link to cancer development, whether it plays an actual role in cancer metastasis remains unclear. It is known, however, to downregulate myosin contractility, a key parameter involved in cell adhesion and migration. We have examined here the potential morphogenetic impact of the high EpCAM expression that characterizes epithelial breast cancer cells, using spheroids of MCF7 cells as model of pre-metastatic cells. We found that EpCAM acted as a repressor of collective migration, while it stimulated single cell migration. Using a combination of cell biological and biophysical approaches, we show that EpCAM depletion globally increased cell contractility, in such a way that the resulting balance of tensions was favorable to cell adhesiveness, resulting in increased tissue cohesion and switch toward collective migration. Most epithelial cells, including MCF7 cells, also express Trop2, a close relative of EpCAM. Intriguingly, we found that Trop2 depletion led to the exact opposite global phenotype from EpCAM depletion, stimulating single cell migration, while decreasing tissue cohesiveness and collective migration. Comparison with EpCAM showed that while both proteins contributed to moderate cell contractility, they differentially modulate the balance of cortical myosin contractility between free edges and adhesive contacts. These differences appeared to rely on subtle differences in the distribution of these two surface proteins. These results highlight the crucial importance of a fine balance of myosin contractility downstream of EpCAM and Trop2, which act as a mechanostat in controlling tissue cohesiveness and in stimulating distinct modes of migration.

Introduction

Contractility of the actomyosin cellular cortex is a central determinant of cell and tissue adhesive and migratory properties. Understanding how contractility is controlled at the global and local scales is thus key to a mechanistic explanation of morphogenetic processes, including during cancer metastasis. In this context, EpCAM is a particularly intriguing candidate regulator. EpCAM, also called TACSTD1, is a cell surface protein specifically expressed in epithelial tissues, and highly overexpressed in most human carcinomas (Rao et al., 2005; Went et al., 2004). It is an important cancer biomarker for diagnostic and therapeutic purposes (Baeuerle and Gires, 2007; Gires and Bauerle, 2010). While the name EpCAM (Epithelial Cell Adhesion Molecule) was given based on its proposed function as a homotypic cell adhesion molecule (Balzar et al., 1999; Litvinov et al., 1994), this function has been strongly questioned by more recent studies (Fagotto and Aslemarz, 2020; Gaber et al., 2018). EpCAM is currently rather viewed as a regulator of intracellular signalling,

impacting on proliferation (Chaves-Pérez et al., 2013; Maetzel et al., 2009) as well as on physical cell properties. The latter activity relies on its ability to downregulate myosin contractility (Barth et al., 2018; Fagotto, 2020a; Gaston et al., 2021; Maghzal et al., 2013; Salomon et al., 2017), providing an obvious putative link between EpCAM and cancer metastasis that remains to be established.

The role of EpCAM in cancer invasion is unclear: In vitro studies have brought conflicting results, consistent with either pro-adhesive or anti-adhesive, pro-migratory or anti-migratory activities (reviewed in (Fagotto and Aslemarz, 2020)). EpCAM is downregulated upon epithelial-mesenchymal transition (EMT) (Pan et al., 2018; Sankpal et al., 2017; Vannier et al., 2013), yet may be itself required for EMT (Gao et al., 2015, 2015; Sankpal et al., 2011; Wang et al., 2018). Of note, the classical view that posed EMT as a necessary and key step in cancer invasiveness is currently a matter of debate. There is emerging evidence that, at least in some cases, the most invasive cells may have only undergone limited EMT, and still display many aspects of the epithelial cells from which they derive (Campbell and Casanova, 2016; Friedl et al., 2012; Jolly et al., 2018). Along these lines, circulating tumour cell lines with high metastatic potential happen to be EpCAM positive (Balcik-Ercin et al., 2021; Koch et al., 2020).

A second related gene, called Trop2 or TACSTD2 is co-expressed with EpCAM in all epithelia, except in the intestine. EpCAM and Trop2 constitute a gene family on their own, Trop2 being the result of the duplication of the EpCAM gene that occurred in reptilians, at the root of amniote evolution. Human EpCAM and Trop2 have high sequence similarity between themselves, and with EpCAM of lower vertebrates. Trop2 has shown identical characteristics to EpCAM in virtually all features examined so far, including structure and biochemical interactions (Fagotto, 2020a; Fagotto and Aslemarz, 2020). Trop2 has been also linked to cancer, but, again, its actual role remains to be established (Fagotto and Aslemarz, 2020; Lenárt et al., 2020; Švec et al., 2022).

EpCAM morphogenetic function is best understood in non-cancer systems, specifically in zebrafish and Xenopus embryos. In both systems, gain and loss-of-function (GOF and LOF) experiments unambiguously showed that EpCAM acts positively on cell-cell adhesion and motility (Maghzal et al., 2010, 2013; Slanchev et al., 2009). In particular, EpCAM is required during gastrulation for ectoderm epiboly, which involves dynamic reorganization of this tissue through cell-cell intercalation (Maghzal et al., 2010, 2013; Slanchev et al., 2009). At later stages of development, loss of EpCAM eventually caused severe defects in tissue integrity (Maghzal et al., 2010, 2013; Slanchev et al., 2009). We showed that all the EpCAM GOF and LOF embryonic phenotypes could be accounted for by its ability to downregulate myosin activity (Maghzal et al., 2010, 2013). At the molecular level, EpCAM directly binds and inhibits the novel class of PKC kinases (nPKC), and through it, it represses phosphorylation of myosin light chain (pMLC) by the

nPKC-PKD-Raf-Erk-MLCK pathway (Maghzal et al., 2013). Importantly, the positive effect of EpCAM on cadherin-mediated adhesion turned out to be a secondary effect of its regulation of myosin contractility (Maghzal et al., 2013). This regulation of myosin via inhibition of nPKC is conserved in human EpCAM (Maghzal et al., 2013). Consistently, EpCAM loss in a rare human intestinal disorder called congenital tufting enteropathy (CTE) leads to disruption of the epithelium (Sivagnanam et al., 2008), due again to myosin overactivation and uncontrolled tension of the actomyosin cortex (Barth et al., 2018; Salomon et al., 2017). Note that a recent study on the migration of isolated intestinal Caco2 cells proposed an additional/alternative role of EpCAM in spatial regulation of RhoA and myosin activity via fast recycling endosomes (Gaston et al., 2021). The significance of this phenomenon in the context of the intact epithelium remains to be evaluated.

Since EpCAM expression is highest in carcinomas, it is fair to predict that its role in controlling myosin activity should be relevant for cancer metastasis. One must emphasize, however, that, due to the multiplicity and complexity of myosin functions, one can hardly predict *a priori* how its up- or downregulation will impact on adhesion and migration in various cell types and under different conditions (Fagotto, 2020a; Fagotto and Aslemarz, 2020). On one hand, contractility of the cell actomyosin cortex is classically viewed as antagonistic to adhesion, as the cortex needs to be softened in order to allow expansion of the interface contacting neighboring cell(s) or the cell matrix (Lecuit and Lenne, 2007; Winklbauer, 2015). On the other hand, cells are also able to respond to increased tension by reinforcing adhesion, which involves further recruitment of adhesive molecules as well as strengthening of the link with the actomyosin cytoskeleton (Leckband and de Rooij, 2014). In turn, both cortical contractility and adhesion have complex effects on cell motility; softening the cell cortex is required for emission of cell protrusions, yet the cortex is also responsible for force transmission, which is also essential for migration, in particular for collective migration (Mayor and Etienne-Manneville, 2016). Adhesion to a support, whether matrix or other cells, is also a basic requirement for most modes of cell migration, yet strong/stable adhesion is bound to slow down and eventually stall migrating cells (Charras and Sahai, 2014).

In an attempt to clarify the role of EpCAM in a cancer context, we chose breast epithelial MCF7 cells as a well-established model of pre-metastatic cells expressing high EpCAM (Osta et al, 2004; Dai et al., 2017). We evaluated the impact of EpCAM levels on the ability of MCF7 cells to migrate as single cells as well as a group, and we systematically characterized the effect on myosin contractility and adhesion, using a combination of cellular and biophysical approaches. EpCAM and Trop2 are thought to be at least partly redundant (Fagotto and Aslemarz, 2020; Wu et al., 2020), and Trop2 expression could partially rescue CTE defects (Nakato et al., 2020). Yet, the

conservation of the two genes throughout amniotes argues for distinct functions, but direct experimental comparison has been missing so far. Thus, while the primary focus of this study was on EpCAM, we thought it important to include Trop2 and characterize both molecules side by side.

We show that, beyond its general role in myosin downregulation, EpCAM differently impacts adhesion and migration depending on the context, here in particular depending on whether cells are isolated or part of a tissue. Furthermore, while our data confirmed that EpCAM and Trop2 share most properties, starting with their common role in inhibiting myosin, we made the unexpected discovery that they actually show counter-balancing contributions to adhesion and motility. The analysis of the cellular and biophysical parameters involved has highlighted how relatively modest differences in the balance of cellular tensions can deeply impact the morphogenetic outcome.

Results

EpCAM depletion increases collective migration of MCF7 spheroids and their cohesiveness

In order to investigate the role of EpCAM in collective migration, we used spheroids of breast cancer MCF7 cells as an in vitro model that mimics a solid tumor (Kramer et al., 2013). These spheroids were placed on a soft matrix of collagen I as a physiologically relevant ECM (Insua-Rodríguez and Oskarsson, 2016). Under these conditions, spheroids actively spread, which we typically imaged over 24 hrs (Fig.1A, Movie 1). We favoured this 2D substrate over spheroids fully embedded in collagen, because in the latter setting, migration also depends on degradation of the extracellular matrix, which would be a confounding parameter here. EpCAM was depleted by transfection of siRNA one day before starting to form the spheroids, which were laid on collagen two days later. By that stage, EpCAM depletion was close to complete and remained so until the end of the assay (suppl. Fig.S1A,C and data not shown). Spheroids formed from cells transfected with control siRNA spread efficiently, typically increasing their area by 3 to 4 folds (Fig.1A,E, Movie 1). Note that the center of the spheroid tended to remain rather compact, while the periphery showed irregular contours, with cells or cell groups frequently sticking out of the cell mass (Fig.1A,H). Non-transfected spheroids behaved identically (not shown). EpCAM knockdown (KD) resulted in a strong, highly reproducible increase in spreading (Fig.1B,E,H, Movie 2). After 24 hrs, spheroids had the shape of a flat pancake, only about 2-3 cells thick (Fig.1H'). Interestingly, these EpCAM KD spheroids expanded as a very cohesive sheet. While numerous protrusions

emanated from the edge of the cell mass (Fig.1H"), this edge was overall strikingly smooth compared to control spheroids (Fig.1H). The distinctive morphologies of control and EpCAM KD, indicative of differences in tissue cohesiveness, were quantitatively expressed as "solidity", a measurement that indicates how closely the surface can be described by a circle (Fig.1F). We validated the specificity of the KD phenotype by showing that it could be fully rescued by re-expression of an EpCAM variant where the siRNA target sequence was mutated (suppl. Fig.S2A). We also verified that the increased migration/spreading of siEpCAM spheroids was not due to a higher proliferation rate by running the spheroid assay in the presence of Mitomycin C (MMC), an anti-mitotic agent (suppl. Fig.S1F). MMC totally blocked the cell cycle, as validated by thymidine analogue EdU incorporation (suppl. Fig.S1F'). We concluded that the increased spreading upon EpCAM KD was independent of cell proliferation, but rather due to changes in morphogenetic properties. In reciprocal GOF experiments, EpCAM overexpression decreased spheroid spreading, thus opposite to the depletion phenotype (suppl. Fig.S2B). One could infer from these results that EpCAM expression in MCF7 cells limits collective migration.

Based on the high sequence and functional similarities between EpCAM and Trop2, and their assumed partial redundancy, one may have predicted that Trop2 could partially compensate for the loss of EpCAM, and that the double EpCAM/Trop2 KD (dKD) would potentiate the EpCAM KD phenotype. To address this question, we also depleted Trop2, using two distinct Trop2 siRNA (sc-43043 and H502-003), which gave very similar results (suppl. Fig.S1B,D,E)(for the rest of the study we used sc-43043). dKD spheroids did not spread more than single EpCAM KD spheroids (Fig.1D,E-H, suppl. Fig.S1E,E', Movie 4). Furthermore, quite unexpectedly, single Trop2 KD decreased spheroid spreading, thus opposite to the effect of EpCAM KD (Fig.1C,E-H, Movie 3). The shape of Trop2 KD spheroids was very irregular, yielding a low solidity value (Fig.1F). Thus, EpCAM and Trop2 appear to play an antagonistic role in this context. While interpretation of double LOF may be ambiguous in such situation, we did include dKD in the following characterization for the sake of completeness, considering the likely possibility that the two molecules may nevertheless share common activities despite their apparent opposition in collective migration.

EpCAM depletion acts via upregulation of myosin activity

As the adhesive and migratory EpCAM LOF phenotypes in Xenopus embryos were due to overactivation of the nPKC-PKD-Erk-myosin pathway (Maghzal et al., 2013), we asked if there was a similar dependency for the effect on MCF7 spheroids. We thus tested the involvement of the key upstream and downstream components of the cascade, nPKC and myosin II, through

treatment with two well-established chemical inhibitors, calphostin and blebbistatin (Fig.2A,B). In the presence of either of these inhibitors, spreading of siEpCAM spheroids was reduced in a dose-dependent manner, close to the levels of controls, while spreading of the control spheroids was further inhibited (Fig.2B). Thus, MCF7 collective migration was indeed positively regulated by nPKC and myosin activity downstream of EpCAM depletion.

We further verified that EpCAM KD stimulated myosin activation, by analyzing phosphorylated myosin light chain (pMLC) in spheroids by whole mount immunofluorescence (IF) (Fig.2C). EpCAM KD indeed significantly increased total pMLC levels compared to controls (Fig.2C,E). The pMLC signal was particularly strong along the free edge of siEpCAM spheroids, suggestive of formation of actomyosin "cables" that could contribute to the smoothness of the circumference (Fig.1B,F and Fig.2C). We also quantified E-cadherin levels, and found them significantly increased in EpCAM KD spheroids (Fig.2D,F), suggesting that cells reacted to increased tension through reinforcement of cadherin-dependent cell-cell adhesion. This reinforcement can be expressed by calculating the E-cadherin to pMLC relative ratio, which tended to be higher in EpCAM KD compared to controls. As we will see below, measurements of tension and adhesiveness for single pairs of cells confirmed this effect.

pMLC was also increased in Trop2 KD, reaching levels comparable to EpCAM KD (Fig.2C,E). E-cadherin levels also tended to increase, but more modestly than in EpCAM KD (Fig.2D,F), and the E-cadherin to MLC ratio was significantly lower (Fig.2G). Thus, while Trop2 KD tissues reached a level of myosin activation comparable to EpCAM KD, high contractility was here less efficiently compensated by cadherin reinforcement. In double KD, neither pMLC nor E-cadherin levels were significantly increased compared to single depletions (Fig.2C-F).

In summary, EpCAM and Trop2 depletions gave a similar global overactivation of myosin, confirming the conservation of their basic function as negative regulator of contractility. Both depletions also led to an accumulation of E-cadherin, indicating that in both cases cell-cell contacts were reinforced in response to increased contractility. We thus faced an apparent contradiction, where depletion of these highly related proteins resulted in diametrically opposite effects on collective migration, despite a similar action on myosin activity and E-cadherin levels. However, differences were observed between the two KD conditions, specifically a more marked peripheral accumulation of pMLC and stronger cadherin reinforcement in EpCAM KD (Fig.2C,G), leading to the hypothesis that subtle differences in intensity and/or localisation of the activity of these regulators may play an important role in the global outcome.

EpCAM and Trop2 KD have opposite effects on single MCF7 cell migration

One obvious possible cause for the spheroid migration/spreading phenotypes could be a difference in the intrinsic migratory property of the individual cells. We analyzed migration of single cells, also plated on a layer of fibrillar collagen I gel. Control MCF7 were moderately motile, with an average motility of 0.5µm/min (suppl. Fig.S3A,E, Movie 5). EpCAM KD cells spread significantly more than controls, adopting a characteristic radial shape with robust protrusions emanating in all directions (suppl. Fig.S3B,G,H, Movie 6). Their migration was drastically decreased compared to control (suppl. Fig.2B,E). Thus, EpCAM depletion, while stimulating collective migration in spheroids, had the opposite effect on single cell migration. On the contrary, Trop2-depleted cells tended to be rounder (suppl. Fig.S3C,F,G, Movie 7) and migrated almost as efficiently as control cells (suppl. Fig.2C,E). dKD cells were closer to EpCAM KD cells, both in terms of spread morphology and low migration (suppl. Fig.2D-H, Movie 8). We could conclude that the differences in collective migration observed upon EpCAM or Trop2 depletion could not be explained by differences in single cell migration capability. However, the degree of spreading of the spheroids was reflected in the morphology of single cells, which suggested a link between the two levels of organization.

EpCAM and Trop2 KD both increase myosin activity, but with different relative impact on cell and substrate adhesive contacts

We hypothesized that the effect of EpCAM (and Trop2) depletion on collective migration resulted from a more complex balance of cellular properties, in particular contractility, cell-cell adhesion and matrix adhesion. We set out to quantitatively characterize the distribution of key cellular components, i.e. pMLC along the actomyosin cortex, E-cadherin at cell-cell contacts, and vinculin as marker of cell-matrix focal adhesions (FAs). pMLC and E-cadherin were analyzed on whole z stacks of confocal images of small groups of cells ranging from 2 to 8 cells (Fig.3 and suppl. Fig.S4). The extreme variability of cell morphologies and contact geometries made it difficult to compare different conditions using standard parameters such as total cadherin or pMLC levels. Instead, since myosin and cadherins tend to concentrate at sites where most tension is exerted, we opted for a determination of the peak intensity for E-cadherin at the cell-cell contact and, for pMLC, at contacts as well as at the free edges exposed to the medium. This approach turned out to be robust over the vast range of cell configurations, and yielded several important results. Firstly, EpCAM KD and Trop2 KD increased all three parameters (Fig.3A,B,C,E), in agreement with data from whole spheroids. Beyond these shared trends were, a comparison between free edges and contacts revealed a clear difference between the two KD conditions. In EpCAM KD, pMLC was

proportionally increased at both locations, as evident from the unchanged contact/edge ratio (Fig.3D). However, in Trop2 KD, pMLC was significantly more increased at contacts (Fig.3C,D). Moreover, while Trop2 KD cells showed the highest E-cadherin intensity (Fig.3E), the pMLC/E-cadherin ratio was also highest under this condition Fig.3F). This suggested that although both EpCAM and Trop2 KD led to higher tension and an apparent reinforcement of E-cadherin adhesion, this latter reaction was proportionally less effective in the case of Trop2 KD, which is fully in agreement with the data on whole spheroids (Fig.2). Phalloidin staining of F-actin followed the same general trend as pMLC (suppl. Fig.S4B,C). dKD cells showed the highest pMLC at the free edge, consistent with a contribution of both EpCAM and Trop2 in moderating contractility, but pMLC and E-cadherin intensities at contacts were low, reflecting a more complex effect of double depletion on cell adhesion (Fig.3D).

We examined cell-matrix adhesive structures using as a marker vinculin, a core cytoplasmic component of focal adhesions (FAs), to which it is recruited in a mechanosensitive manner. We performed this analysis on single cells (Fig.3G), to uncouple it from the impact of cell-cell adhesion. The total vinculin intensity at FAs (Fig.3H) was further normalized to the ventral cell surface, to account for the large differences in cell spreading of control, EpCAM and Trop2 KD cells (Fig.3H'). We found that the total FA signal tended to increase for both EpCAM KD and Trop2 KD, and was highest for dKD (Fig.3G,H), similar to the trend observed for cortical pMLC. Interestingly, when normalized to the cell surface, the signal in EpCAM KD cells was similar to that of control cells, while it was significantly stronger in Trop2 KD (Fig.3H'). Thus, it appeared that upon EpCAM depletion, FA strengthening and cell spreading balanced each other, while in the case of Trop2 KD, tension on the substrate was proportionally more acute.

Altogether, this analysis confirmed at the single cell level that depletion of either EpCAM of Trop2 boosted myosin activation. However, there were key differences in the effects of depletion of the two genes, which suggested that upon loss of EpCAM, increased contractility was tuned toward favoring cell spreading and high tissue cohesiveness, while in Trop2 KD, tension was proportionally higher at contacts, consistent with lower cohesiveness.

Cell-substrate and cell-cell forces are elevated upon EpCAM and Trop2 depletion

These observations prompted us to measure the actual forces exerted on these different structures. In a first approach, we used traction force microscopy (TFM) on cell pairs adhering to H micropatterns (Fig.4A). This method had unique advantages for our purpose: The H patterns constrained the cell pair to adopt a stable configuration, providing a robust system to directly

measure traction exerted on the matrix and, at the same time, to indirectly calculate the force at the cell-cell contact, simply based on the counterbalance of forces (Fig.5A')(Tseng et al., 2012). A bonus from this technique was that the H pattern, by imposing a fixed geometry and a limited surface for the contacts to the matrix (Fig.3B), partly solved a major challenge, i.e. the wide differences in cell morphology of cells on non-constrained collagen substrate, naturally observed within the wild type MCF7 cell population, and further exacerbated by EpCAM and Trop2 depletions.

EpCAM KD caused a significant increase of the total contractile energy, reflecting a strong traction exerted on the FA (Fig.4C,D). These results directly demonstrated the increased contractility in EpCAM KD cells, confirming the pMLC IF data. The global force exerted on the cell-cell contact, Fcc, was also increased, an expected result of high global cell contractility (Fig.4E). Yet, the length of cell-cell contacts, which is a readout of adhesiveness (see below), was significantly broader for EpCAM KD pairs (Fig.4B,G). This result was again consistent with EpCAM-depleted cells responding to increased contractility by cadherin recruitment and reinforcement of cell-cell adhesion.

Trop2 KD also increased both total contractile energy and cell-cell forces (Fig.4C,D,E). However, contact length was only marginally increased (Fig.4B,G), supporting, together with the IF data, the notion that, while both EpCAM and Trop2 depletions upregulate myosin-dependent cortical tension, adhesion reinforcement in Trop2 KD cells was less efficient. As expected, double depletion also increased contractile energy, yielding the highest cell-cell force and highest cell-cell to total force ratio, consistent with EpCAM and Trop2 both contributing to moderating myosin contractility in these cells (Fig.4E,F).

The substrate used for TFM was a thin layer of collagen coated on acrylamide. We verified collective migration of spheroids on this acrylamide-based substrate. We found essentially the same phenotypes as on fibrillar collagen gel: EpCAM depletion strongly increased spheroid spreading, while maintaining high cohesiveness as indicated by high solidity values (suppl. Fig.S5).

EpCAM KD modulates cortical tension and adhesiveness in substrate-free cell doublets

Our TFM data provided a simultaneous quantitative measurement of cell-matrix and cell-cell adhesion. Since both types of adhesions are likely to influence each other, we also wanted to evaluate changes in cortical tension and in cell-cell adhesiveness in the absence of cell matrix adhesion. These parameters can be accurately measured simply based on the geometry of free cell doublets laid on a non-adherent surface (Canty et al., 2017; Fagotto, 2020b; Winklbauer, 2015).

Such doublets adopt a typical configuration, where the cell contact expands until contact tension γ_c, ($\gamma_{c(AB)}$ in the diagram of Fig.4H) is precisely balanced by the cortical tension at the interface with the medium γ_m). Furthermore, if the two cells differ in their cortical tensions ($\gamma_{m(A)}$ and $\gamma_{m(B)}$, Fig.4H), the doublet adopts an asymmetric geometry, as the softer cell tends to engulf the stiffer cell (Fig.4H). The relative value for the three tensions, $\gamma_{m(A)}$, $\gamma_{m(B)}$ and $\gamma_{c(AB)}$ can be directly deduced from the geometry of the membranes at the contact vertex (Canty et al., 2017; Fagotto, 2020b; Kashkooli et al., 2021) From these measurements, two important information can be extracted: a) The relative cortical tensions γ_m of the two cells, expressed as $\gamma_{m(A)}/\gamma_{m(B)}$, and b) the $\gamma_{c(AB)}/\gamma_{m(A)}$ ratio, which directly reflects the state of adhesion of a contact. A convenient way to express this relationship is "adhesiveness" (Parent et al., 2017), an absolute number between 0 and 1, which is inversely related to the γ_c/γ_m ratio (Fig.4L) and positively related to contact length (Fig.4G).

We adapted the protocol previously used for embryonic cells (Canty et al., 2017; Kashkooli et al., 2021; Rohani et al., 2014) to mildly dissociate MCF7 monolayers into single cells, which we mixed at low density to favour formation of both homotypic and heterotypic doublets, which we imaged by confocal microscopy (Fig.4I,J). We systematically analyzed the effect of single and double EpCAM and Trop2 KD cells and made the following observations.

Firstly, heterotypic doublets made of a control (A) and a manipulated cell (B) were clearly asymmetric (Fig.4I), corresponding to a Ct_A/Ct_B significantly lower than 1. This constituted a firm demonstration that cortical contractility was indeed increased upon EpCAM and Trop2 KD (Fig.4K). Second, contact angles of homotypic doublets were less acute for EpCAM KD than controls (Fig.4J), corresponding to a significant increase in adhesiveness (median 0.58 compared to 0.40 for controls (Fig.4L). In the case of Trop2 KD, however, only a small, non-significant increase was observed (Fig.4L). dKD doublets were similar to EpCAM KD (Fig.4L). These two results were in perfect agreement with IF and TFM data, demonstrating that while both KD led to increased contractility, only EpCAM KD efficiently boosted adhesiveness.

Spheroid spreading phenotypes can be simulated based on cell properties

We asked whether our characterization of contractile and adhesive properties could account for the striking differences in the behaviour of the spheroids. A simple description of the system can be made based on the tensions exerted along the three cell interfaces (Fig.5A-C), i.e. tension along the free edge exposed to the medium (γ_m), at the cell-cell contacts (γ_c), and lastly at the cell-extracellular matrix interface (γ_x). As described above, the relative strength of the cell-cell tension γ_c and of the cell-medium tension γ_m determine adhesiveness. One key observation in this study

was that EpCAM KD cells had higher adhesiveness than control cells (Fig.4G,L), despite being much more contractile (Fig.4D,K). This effect was explained by the stronger increase in γ_m relative to γ_c (Fig.5A,B). In the case of Trop2 KD cells, both γ_m and γ_c were also increased, but their relative values were roughly maintained, such that there was no significant change in adhesiveness (Fig.4G,L and Fig.5B).

Spreading on the extracellular matrix can be similarly described based on γ_m and γ_x, which are counterbalanced by the tension of the elastic substrate γ_s (for simplification, we consider here only the horizontal component, which corresponds to the TFM readout)(Fig.5C). This balance of force can be expressed as $\gamma_s = \gamma_x - \gamma_m * \cos(\Phi)$. As consequence of this relationship, if $\gamma_s = \gamma_x$, the edge of the cell forms a right angle with the substrate. For $\gamma_s - \gamma_x < 0$, the cell spreads more on the substrate, forming an acute angle Φ, while on the contrary, for $\gamma_s - \gamma_x > 0$, Φ is obtuse, thus the cell tends to contract. These three situations corresponded to the conditions that were used in our experiments, respectively controls, EpCAM KD and Trop2 KD (Fig.5A,C). The correspondence was supported by the comparison between γ_s and the total contractile energies from TFM (Fig.4D), by the xz projections of the single cells (suppl. Fig.S4F,G), and by the vinculin data (Fig.3G,H), which were qualitatively consistent with relative γ_x values.

With these cellular parameters at hands, we thought to simulate spheroid spreading using a cellular Potts model (Glazier and Graner, 1993; Graner and Glazier, 1992), specifically a 3D version (CompuCell3D (Cickovski et al., 2005; Izaguirre et al., 2004)). In this model, the "tensions" for a given cell type are input as relative "energies" (see appendix). While these energies are arbitrary values, they are related to γ_m for the cell-medium energy, γ_c for cell-cell energy, and γ_x-γ_s for cell-matrix energy.

We considered an initially compact group of cells laid on a flat surface, and set the three energies (Fig.5G) to fit our data on single cells and cell doublets (suppl. Fig.S4H,I and annex, qualitative summary Fig.5A-C). The key features were (1) higher global energy for both EpCAM KD and Trop2 KD, which accounted for increased contractility compared to controls, nuanced by specific differences between the two depletions, (2) a lower cell-cell energy/cell-medium energy ratio (thus higher adhesiveness) for EpCAM KD, as well as (3) a cell-substrate energy set negatively for EpCAM KD, and positively for Trop2 KD, consistent with their respective spreading and contracting properties. Simulation of the behaviour of spheroids under these three conditions yielded clear differences in the degree of spreading, moderate for the control condition, high for EpCAM KD, and very low for Trop2 KD (Fig.5D-F, H, Movies 9 and 10), which faithfully reproduced the experimental spheroid spreading phenotypes (Fig.5D'-F', H'). Note that we

purposely chose to perform simulations that only considered the three cellular tensions. Indeed, the goal was to highlight the explanatory power of a simple model based on the relative strengths of these basic parameters, which could recapitulate very well the spreading phenotypes. The simulations did not fully mimic more detailed aspects of the spheroid morphology, in particular the convoluted outlines of the Trop2 KD spheroids (Fig.5F,F'), which would require to complexify the model with additional parameters, e.g. properties of protrusions. In summary, we show here that the experimentally observed differences in distribution of cortical contractility are sufficient to account for the diametrically opposite behaviours produced by EpCAM and Trop2 depletions.

Subtle differences in subcellular distribution of EpCAM and Trop2 may account for the distinct phenotypes

In an attempt to understand the cause for the different cell behavior caused by EpCAM and Trop2 depletions, we compared the localization of the two proteins by IF (Fig.6). We analyzed small groups of cells, which offer a conveniently simple configuration for quantitative analysis. Both EpCAM and Trop2 were found all along the plasma membrane, including cell-cell contacts. Under standard IF conditions with permeabilization, some EpCAM and/or Trop2-positive intracellular spots were observed (suppl. Fig.S6D). Here, we focused on the pools exposed at the plasma membrane by performing IF on non-permeabilized cells. We quantified the distribution along various plasma membrane locations, in particular dorsal and ventral membranes, and cell-cell contacts. These three main locations corresponded to the sites where the three basic tensions are exerted, respectively γ_m on the dorsal side, γ_x at the ventral matrix interface, and γ_c at cell-cell contacts. Additional subregions were defined for a more detailed analysis (suppl. Fig.S6). Altogether, the two molecules had a very similar distribution (Fig.6C for major regions, suppl. Fig.S6 for full analysis), as one may expect for closely related proteins. Interestingly, the ventral side showed the lowest levels (compared notably to the dorsal side), yet Trop2 was comparatively more abundant than EpCAM at this location (Fig.6B). The resulting difference in dorsal/ventral ratio was modest (~20%) but highly reproducible (Fig.6D).

In order to predict the potential impact of either EpCAM or Trop2 depletions on the three cortical tensions, one had to consider the complexity of the system involving co-expression of two regulators with similar yet not identical activities. Thus, while the loss of EpCAM will increase contractility, one must keep in mind that the cells still express Trop2, of which the particular distribution will contribute to the new balance of tensions. The reciprocal scenario applied to Trop2 KD. It was thus essential to determine whether EpCAM and Trop2 distributions were sensitive to the loss of the other protein. It turned out that upon EpCAM KD, Trop2 levels were significantly

decreased in most locations (Fig.6C and suppl. Fig.S6). Thus, EpCAM KD cells experienced not only the loss of EpCAM, but also a partial loss of Trop2. One notable exception was the ventral side, where Trop2 levels were on the contrary increased (Fig.6C). This local enrichment was significant, as it shifted the balance between the dorsal and ventral sides (Fig.6E). Boosting the inhibitory action of Trop2 was predicted to locally dampen myosin activity at the matrix interface of cells that were otherwise globally more contractile. In terms of tension, this implied that the γ_x/γ_m ratio would decrease, thus likely to contribute to increased spreading of the cell on the substrate (see Fig.5A,C). Note another consequence of EpCAM depletion on Trop2 distribution, which led to a significantly lower ratio between the dorsal side and cell-cell contacts (Fig.6E). This feature was also predicted to decrease γ_c/γ_m, and thus to favour cell-cell adhesion (Fig.5G).

The situation was different in the case of Trop2 KD, as EpCAM appeared largely unaffected. One could then infer that myosin upregulation was here mostly dependent on the depletion of Trop2, while the normal regulation by EpCAM was maintained. What was here particularly relevant for the prediction of changes in tension was the moderating action due to the relative enrichment of Trop2 in control cells (Fig.6C,D). As a consequence, while Trop2 depletion did cause a global upraise in contractility, the effect would be expected to be even more pronounced at this interface (Fig.6G), thus increasing the γ_x/γ_m ratio. As this effect would not be here compensated by EpCAM, it would account for the decreased contact area with the substrate (Fig.5 and Fig.6G).

In summary, while in wild type cells EpCAM and Trop2 have largely the same distribution, and probably contribute in a similar manner to set the balance of tensions, they differ in several major aspects (Fig.6G): Firstly, Trop2 levels are dependent on EpCAM, but not vice versa. Secondly Trop2 appears to be slightly more expressed along the substrate interface, where it is further enriched upon EpCAM depletion. A similar shift in balance was measured for cell-cell contacts. As discussed below, the simple partial shift in their relative distribution could explain the surprisingly opposite phenotypic outcomes in terms of collective migration.

Differences in polarization may account for differences in single cell migration

The opposite effect on single versus collective migration was not fully intuitive. In particular, the rounded morphology of Trop2 KD cells (suppl. Fig.S3) and the strong vinculin enrichment at FAs were not a priori typical signs of migratory cells (Fig.3H-I). Yet, one general difference that was consistent with the single cell migration phenotypes could be found in the arrangement of the protrusions and of the associated FAs (suppl. Fig.S7). Cells displayed a variety of morphologies, which we compiled into five categories reflecting both the degree of spreading and

symmetry/asymmetry, as indicated in suppl. Fig.S7F, with examples provided in suppl. Fig.S7A-D. Control cells displayed a wide range of spreading, but the majority of them had FAs distributed in asymmetric patterns (suppl. Fig.S7C). EpCAM KD cell, on the other hand, did not only spread quite extensively, but FAs were, in the vast majority of cases, arranged in strikingly radially symmetric patterns (suppl. Fig.S7A,B). In Trop2 KD cells, even though the substrate interface was generally round, with FAs arranged as a peripheral ring, the symmetry was broken in most cases, either through a gap in the FA ring (suppl. Fig.S7D, filled and concave arrowheads), or emission of a dominant protrusion that conferred a unipolar configuration (suppl. Fig.S7E). These observations argued that highly spread cells tended to adopt a stable radial configuration, while cells with a smaller contact area were more prone to a break of symmetry that allowed effective migration.

EpCAM expression favours escape of individual cells from spheroids

MCF7 cells are considered to display high cell-cell adhesion and low migration, characteristic of epithelial cells. Consistently, spheroids spread as a compact cell mass. Yet, a close look at our time lapses of wild type spheroids showed occasional detachment and migration of individual cells (Fig.7A, Movie 11). We found that 25 out of 84 control spheroids (from 13 experiments) had at least one isolated cell that detached and migrated away over the first 24 hr of imaging, and 7 additional spheroids even showed detachment of small groups of cells (Fig.7E). EpCAM KD (Fig.7B, Movie 12) appeared to drastically repress such events (only three cases of detachment for 85 spheroids, Fig.7E). The frequency of cell detachments was higher with Trop2 KD spheroids, here cells leaving mostly as small groups (Fig.7E, a pair of cells in the example of Fig.7C and Movie 13). Detachments were rare in dKD (Fig.7D,E, Movie 14). The same phenomenon of EpCAM-dependent single cell detachment was also observed for spheroids laid on collagen-coated polyacrylamide (suppl. Fig.S5). These results indicated that EpCAM expression favoured cells breaking out of the compact cell mass. Even though these events were rare for this particular cell line under the conditions used experiments, the repressive effect of EpCAM may be relevant for cancer invasion.

Discussion

We uncovered in this study an unexpectedly subtle regulatory system that has a major impact on adhesive and migratory properties: On one hand, EpCAM and Trop2 show almost identical properties. In particular, they both similarly act as negative regulators of myosin activity, working

toward the same goal of moderating global cell contractility. Nevertheless, at least in the model of breast cancer MCF7 cells, depleting one or the other leads to diametrically opposed phenotypes, indicating that this quasi twin pair of molecules functions as a mechanostat of tissue morphogenesis.

By accurately dissecting this system at the tissue and single cell level, we succeeded at solving at least part of this puzzle, showing how relatively small variations in the balance of cellular tensions can have a large effect on the final behavioral output. Thus, while global tension increases in both EpCAM KD and Trop2 KD, the ratios between γ_m, γ_c and γ_x differ in such a way that EpCAM KD favours cohesive tissue spreading, which is on the contrary repressed by Trop2 KD. An important characteristic of this dual EpCAM-Trop2 system that became obvious in our experiments, is that interpretation of the LOF phenotype of one of the two components must take into account the activity of the remaining partner. This was particularly striking in the case of EpCAM KD, which also affected Trop2 levels and distribution, which in turn influenced the adhesive and migratory phenotype. This is a key concept that needs to be considered when examining the role of EpCAM and Trop2 in various tissues. One should also stress that the LOFs of EpCAM or Trop2 achieved in this study were rather acute (over a couple of days). It is conceivable that, on the longer term, the remaining partner may adapt to this loss, which would explain the apparent redundancy observed in mouse single knock-out experiments (Guerra et al., 2012; Lei et al., 2012; Wang et al., 2011).

Our previous results from LOF and GOF experiments in Xenopus embryos were all consistent with EpCAM acting as a positive regulator of cell-cell adhesion. However, one must emphasize that the effect on cadherin adhesion was indirect, as it resulted from the repressive activity of EpCAM on myosin contractility (Maghzal et al., 2010, 2013). Thus, the dramatic tissue disintegration, which was the end result of EpCAM depletion in these embryos, was a consequence of myosin overactivation, which led to decreased cell-cell adhesion and to loss of cadherin (Maghzal et al., 2013). This scenario was fully consistent with the antagonistic action of cortical tension on adhesion as described in the classical biophysical models (Brodland, 2002). However, cortical actomyosin contractility has additional roles. In particular, it is also essential to stabilize and reinforce adhesion (Charras and Yap, 2018). Considering this complexity, we predicted that the negative role of EpCAM on myosin may not always be pro-adhesive, but could lead to divergent outcomes depending on multiple factors, such as EpCAM levels, activity of the nPKC-dependent pathway, basal level of cortical contractility, and a variety of other parameters (Fagotto and Aslemarz, 2020; Maghzal et al., 2013). We now show that in MCF7 cells, EpCAM KD indeed

increases cell adhesion and tissue cohesiveness, thus opposite to the loss of adhesion in embryonic tissues. We suggest that the anti-adhesive facet of contractility dominates in the early Xenopus embryonic tissues, while the cytoskeleton of MCF7 cells is in a regime more compatible with efficient reinforcement of adhesive contacts. One consequence of this situation is that cell-cell contacts can cope with rather large changes in cell contractility, as experienced upon EpCAM or Trop2 depletion. Note that, while "adhesiveness" is only significantly upregulated in EpCAM KD (Fig.4L), the global force that cell-cell contacts withstand is high in both EpCAM and Trop2 KD (Fig.4E).

These observations highlight the spectrum of properties that can be achieved based on differential regulation of local cortical tension. In MCF7 cells, the system appears to be set in such a way that the cell and tissue behaviour can be tilted one way or the other in response to relatively subtle differences in the balance of contractility under the differential control of EpCAM and Trop2. Future investigations will be required to determine the molecular basis of EpCAM and Trop2 specificities. Potential parameters may include association with membrane microdomains, interactions with the cytoskeleton, and/or differential stability and/or endocytic routes (Fagotto and Aslemarz, 2020; Gaston et al., 2021; Kuhn et al., 2007; Nubel et al., 2009). Without excluding potentially distinct activities of EpCAM and Trop2, our data support a simple model where their partial enrichment at specific sites produces differences in local tensions, which may be sufficient to account for their differential effect on adhesion and migration.

Simple considerations on the relative impact of the three tensions γ_m, γ_c and γ_x provides an explanatory logic for most situations, including the different effects of EpCAM/Trop2 KD on single cells and spheroids. In the simple case of isolated cells, a large portion of their surface exposed to the medium, the rest being in contact with the matrix. Their behaviour is then controlled by γ_m and γ_x. In a cell mass, however, a large fraction of the cells is buried in the core, fully surrounded by other cells, thus γ_c dominates. Only those cells exposed to the surface are under the influence of the γ_c/γ_m balance. Cells at the base of the spheroid are subjected to γ_c and γ_x, and those at the edge of the spreading spheroid to all three tensions. This is sufficient to explain why the core of the wild type spheroids remains compact, while cells at the edge can bulge out and even detach, driven by their ability to migrate on the matrix. It also explains the differences in the effect of EpCAM KD for single cells and spheroids: For the former, high spreading and increased cortical tension favoured formation of radially oriented protrusions pulling symmetrically in all directions, which led to their immobilization. In spheroids, the fact that the same EpCAM-depleted cells actively moved as a group can be readily explained by polarization of the cells at the margin, due

to the inevitable asymmetry between their edge, exposed to the medium, and the cell-cell contacts. Such asymmetry is a well-established feature of collective migration (Mayor and Etienne-Manneville, 2016).

We consider that the depletion/overexpression approach used in this study, although obviously prone to caveats inherent to LOF/GOF experiments, had here a clear physiological relevance, since the magnitude of the changes in EpCAM and Trop2 levels was compatible with what happens during cancer development. MCF7 cells represent in this regard a good model, based on the elevated expression levels compared to normal epithelia as well as on the abrupt drop in EpCAM expression observed after triggering EMT (Sankpal et al., 2017). While this study has only addressed the function of EpCAM and Trop2 in a specific cell line in an *in vitro* context, we hypothesize that co-expression of EpCAM and Trop2 may act as a general mechanostat contributing in setting the adhesive and migratory properties, which may be broadly relevant in the context of the biology of carcinoma. Our data highlight their capacity to elicit distinct behaviours under different situations. For instance, changes in their expression is predicted to differentially affect cells located within a tumour and cells positioned at its edge. In the latter case, the presence of EpCAM and/or Trop2 may well be pivotal for the fate of those cells that, in response to other parameters, may be already on the verge of escaping. Similarly, for cells that have already undergone invasion, the impact of EpCAM and Trop2 expression will differ for single cells versus groups of cells undergoing collective migration. In this context, we find it particularly intriguing that EpCAM expression promotes cell escape from a compact tissue, and that Trop2 depletion in an EpCAM-positive tissue favours detachment of cell groups. While such events were only observed at low frequency in the non-invasive MCF7 cell line, EpCAM could play a more prominent role under conditions corresponding to the early stage of transition to metastasis. How the morphogenetic potential of EpCAM is integrated with the multiple other factors that influence tensile forces, adhesion and motility is an exciting topic for future studies.

Material and methods

Cell culture. MCF-7 cells, originally acquired from ATCC, were provided by the SIRIC Montpellier center. They were grown in complete culture medium, i.e. Dulbecco's modified Eagle's medium (DMEM) with 4.5 g/l glucose, supplemented with 10% fetal bovine serum (FBS), 1% antibiotic-antimycotic and 1% non-essential amino acids (all Gibco/Thermo Fischer Scientific), at 37°C and 5% CO_2, for a maximum of 10 passages. 0.05% Trypsin-EDTA (Gibco/Thermo Fischer Scientific) was used for dissociation and passage.

Antibodies, reagents, and solutions. The list of antibodies and dilutions used for IF are presented in Table 1. Secondary antibodies and phalloidin conjugated to Alexa fluorophores were from Molecular Probes/Thermo Fischer Scientific. EpCAM (sc-43032), Trop2 (sc-72392) and control non-targeting (sc-37007) siRNA were from Santa Cruz Biotechnology. A second Trop2 siRNA (H502-0033) was obtained from Sigma/Merck. Mitomycin C was from Sigma/Merck (M4287). Calphostin and Blebbistatin from EMD/Millipore. The EdU click reaction kit with Alexa Fluor 488 dye was from Invitrogen/Thermo Fisher Scientific (C10337). Phosphate Buffer Saline (PBS) without calcium and magnesium was from EuroBio (CS1PBS01-01). Tris Buffer Saline (TBS) was 100mM Tris-HCl pH 7.2, 150mM NaCl. Dissociation buffer was 88mM NaCl, 1mM KCl and 10mM NaHCO3, pH = 9.5 (Canty et al., 2017).

Table 1. List of antibodies

Antigen	Antibody name	Species	Supplier and cat #	Dilution
EpCAM	323/A3	Mouse	Sant Cruz Biotechnology	1:1000
Trop2	MA5	Rabbit	MA5-29593, Invitrogen	1:1000
pMLC	(Ser19) pMLC	Mouse	3675, Cell Signaling	1:200
pMLC	(Ser19) pMLC	Rabbit	AB3381, Millipore	1:1000
E-cadherin	24E10	Mouse	3195, Cell Signaling	1:400
vinculin	MA1103	Mouse	Boster Bio	1:100

siRNA transfection. Cells were seeded in 24-well plates at 0.2×10^6 density one day before siRNA transfection, and 1.6ml fresh medium was added just before transfection. 40 picomoles siRNA (2x 40 picomoles for dKD) and of 4µl Lipofectamine RNAiMAX (8µl for kD) (Invitrogen/Thermo Fischer Scientific) were added to each well. Efficient KD was obtained after 48 to 72 hours.

Fibrillar collagen gels. Glass bottom dishes (Cellvis, D35-20-1.5-N) or 12mm round coverslips were plasma cleaned to create a hydrophilic surface, then coated at 4°C with a thin layer of a 2mg/ml solution of collagen I (from a ~3mg/ml stock solution in 0.02N acetic acid) in PBS, titrated to alkalinity by addition of NaOH, and incubated at 37 °C for 30 min for gelling.

Spheroid formation. The siRNA transfected cells were dissociated by trypsin and counted using trypan-blue solution and an automated cell counter (Invitrogen, Countess). For each spheroid, 400 cells were suspended in 200 µl complete culture medium containing 20% methylcellulose (Sigma, M0262-100G) and incubated in single wells of round-bottom 96-well plates (Greiner Bio-One Cellstar, 650185) for 48hrs.

Spheroid migration assay. The formed spheroids were transferred to glass-bottom dishes coated with collagen gel. Adherence to the gel was observed within 30 min. Spheroids were imaged with

an Olympus IX83 inverted widefield video-microscope controlled by Metamorph software using a 10x (0.3NA) or 20x (0.45NA) objective. Time lapse images were acquired every 30 min for 24hrs.

Single cell migration assay. Cells were dissociated in dissociation buffer and counted as above, 0.5×10^5 cells were plated on top of collage gel and left to adhere for about 3 hours before acquisition of time lapses. Imaging conditions were as for spheroids, with a 20x (0.45NA) objective, every 5 to 7 min for 6 hours.

Immunostaining. Spheroids (in glass-bottom dishes) were fixed for 30 min in 3.7% paraformaldehyde (PFA, #15714, Electron Microscopy Sciences) in PHEM buffer (60mM PIPES, 25mM HEPES, 10mM EGTA, and 4mM MgSO4, pH 7.2), followed by 30 min permeabilization in 1% Triton X100 in PBS. Fixed samples were washed twice with TBS, incubated for 45 min at RT in blocking buffer (20% sheep serum (S2350-100, Biowest) in PBS, followed by overnight at 4°C with primary antibodies and fluorescent phalloidin diluted in PBS with 10% sheep serum, then another overnight with secondary antibodies and Hoechst 33342 (H3570, Invitrogen/Thermo Fischer Scientific, 1:2000), rinsed and kept in PBS. Fixation and immunostaining of cells and groups of cells (on coverslips) were similarly, but with shorter times (10 min fixation, 10 min permeabilization, 1-2 hrs incubation with antibodies, all at RT), and coverslips were mounted using antifade mounting media (Slowfade, S36972, Molecular Probes/Thermo Fischer Scientific). For cell-surface labelling, Triton X100 permeabilization after fixation was skipped, but samples were post-fixed after primary antibody incubation, and permeabilized before incubation with the secondary antibodies.

Confocal microscopy. z-stacks (0.2 to 0.4µm distance between planes) of immunolabelled cells and groups of cells were acquired using an inverted scanning confocal microscope (Leica SP5-SMD), 63x oil objective (1.4NA). Spheroids were imaged using a Nikon inverted microscope coupled to the Andor Dragonfly spinning disk, 40X water objective (1.15NA) as z-stacks of 4 by 4 tile-scans (1µm distance between planes), which where stitched to generate full images of whole spheroids.

Image quantification

All quantifications were performed using ImageJ. For measurement of relative E-Cadherin and pMLC signal intensities of whole-mount labelled spheroids, the membrane signal was obtained from horizontal confocal slices through thresholding after background subtraction. Values were normalized for each experiment to the average signal in control spheroids. For small groups of cells, peak intensities for pMLC and E-cadherin were measured by drawing a line across two

adjacent cells, and running the corresponding plot profile function throughout the z stack to select the planes with respectively highest E-cadherin and pMLC peaks at cell-cell contact, and highest pMLC peaks at each free edge. These measurements were repeated for each cell pair of a group. Relative intensities were calculated from the areas of these peaks after background subtraction. EpCAM and Trop2 relative signals in cell groups were measured as average intensity on line scans drawn along the plasma membrane at defined locations, either on horizontal sections or on z projections produced using the "reslice" function. The detailed locations are detailed in suppl. Fig.S6.

Traction force microscopy. Stock solution for soft polyacrylamide substrates of 5 kPa rigidity containing far-red fluorescent nanobeads (Bangs laboratory, FC02F, 0.19 μm) were prepared by mixing acrylamide 40% (A4058, Sigma) and bis-acrylamide 2% (M1533, Sigma) in DPBS 1X (PBS without Ca & Mg, CS1PBS01-01, Eurobio Scientific) according to documented relative concentrations (Tse and Engler, 2010; Vignaud et al., 2014). The thin polyacrylamide-based substrate was polymerized between two different glass coverslips (#631-0162, diameter 32 millimeters, thickness No. 1, VWR) prepared as follows. The first coverslip served as base for the gel. It was cleaned using a plasma cleaner machine, then coated with bind-silane (#GE17-1330-01, Sigma) for 3 to 5 min at RT to ensure the attachment of the gel to the coverslip. The second coverslip served to transfer the patterned extracellular matrix. It was also first plasma cleaned, then coated with 0.1 mg/ml PLL-PEG (PLL20K-G35-PEG2K, JenKem Technology) solution for 30 min at RT to obtain a passivated surface. It was then washed with distilled water, dried, then burned for 5 min with UV light through a micropatterning chrome photomask (45 by 45 μm custom-designed H shapes, micropatterned onto chrome photomask by Toppan). This allowed adsorption of the collagen coating at the burned sites resulting in a micropatterned coated coverslip. Collagen type-I was added at 0.5mg/ml in 0.02 N acetic acid and left for 45 min at RT. For gel polymerization, 1 μl of 10% ammonium persulfate (A3678, Sigma), 1 μl of TEMED (T9281, Sigma) and 0.35 μl of the above-mentioned nanobeads were added to 165 μl of the acrylamide-bisacrylamide stock solution. 47 μl of this solution were used to put between the two coverslips for polymerization (30 min, RT). Once polymerized, the collagen-coated top coverslip was gently removed, exposing the collagen H micropatterned gel. Cells were plated on this substrate at a density of 0.5×10^5 per coverslip in a culture dish. The medium of each dish was replaced with fresh medium to wash out cells that didn't adhere to the substrate (this step avoided ending up with cells that were not on the patterns). The dishes were then kept in the incubator overnight to allow cell division to obtain cell doublets on each H micropattern. Cells and the underneath nanobeads were imaged using an epifluorescence inverted microscope (Nikon Ti2-E2) with 40x air

objective (1.15NA) and an Orca Flash 4.0 sCMOS camera (Hamamatsu), with temperature set at 37°C. This first image served as stressed (pulled) state of the beads. Then the cells were removed from the patterns using trypsin and another image of the same position was taken serving as unstressed state of the beads. The displacement field analysis was done using a custom-made algorithm based on the combination of particle image velocimetry and single-particle tracking. Traction forces were calculated using Fourier transform traction cytometry with zero-order regularization (Milloud et al., 2017; Sabass et al., 2008). All calculations and image processing were performed using MATLAB software.

Production and analysis of free-floating cell doublets. siRNA transfected cells were dissociated by a 10 min incubation at RT with dissociation buffer. The buffer was then removed, 1 ml of complete culture medium was added to the cells, and single dissociated cells were obtained by pipetting. Dissociated cells of two different conditions (with control cells labelled with Hoechst 33342) were gently mixed, transferred to agarose-coated plastic dishes (2% agarose in PBS) in complete culture medium and put in the incubator for 10 to 15 min to allow partial reassociation. Reassociated cells were then gently transferred to a glass-bottom dish coated with a thin layer of 2% agarose, in complete culture medium containing a 1:10000 dilution of the membrane dye CellMask deep red (C1004, Molecular Probes/Thermo Fischer Scientific). Cell doublets were imaged by live confocal microscopy using a Dragonfly spinning disk (Andor) mounted on a Nikon inverted microscope with a 20x (0.75 NA/oil) objective, at 37°C and 5% CO_2. Hoechst and CellMask images were obtained simultaneously using two CCD cameras (EMCCD iXon888 Life Andor). Quantifications of the relative cortical tensions and adhesiveness were done based geometry of cell membranes at the vertices, as previously described (Kashkooli et al., 2021). Homo- and heterotypic doublets were identified based on the presence of Hoechst-positive nuclei.

Statistical analysis. All statistical analyses were performed using the Excel real statistics add-in. Unless otherwise stated, experiments were replicated at least three times and comparisons between conditions were done using either one-way ANOVA followed by Tukey-HSD post hoc test, or the non-parametric Kruskal-Wallis Test, followed by Dunn post-hoc test. p values met the following criteria $*p < 0.05$, $**p < 0.01$, and $***p < 0.001$ and NS, not significant.

Acknowledgements

This study was supported by ANR grant ANR-14-ACHN-0004–ICM, a Labex EpiGenMed Chair of excellence ANR grant to F.F., and CIHR grant 130350 to F.F. and P.L.

References

Baeuerle, P.A., and Gires, O. (2007). EpCAM (CD326) finding its role in cancer. British Journal of Cancer *96*, 417–423. https://doi.org/10.1038/sj.bjc.6603494.

Balcik-Ercin, P., Cayrefourcq, L., Soundararajan, R., Mani, S.A., and Alix-Panabières, C. (2021). Epithelial-to-Mesenchymal Plasticity in Circulating Tumor Cell Lines Sequentially Derived from a Patient with Colorectal Cancer. Cancers (Basel) *13*, 5408. https://doi.org/10.3390/cancers13215408.

Balzar, M., Winter, M.J., de Boer, C.J., and Litvinov, S.V. (1999). The biology of the 17–1A antigen (Ep-CAM). Journal of Molecular Medicine *77*, 699–712.

Barth, A.I.M., Honesty, K., and Riedel-kruse, I.H. (2018). Regulation of epithelial migration by epithelial cell adhesion molecule requires its Claudin-7 interaction domain. 1–24. .

Brodland, G.W. (2002). The Differential Interfacial Tension Hypothesis (DITH): a comprehensive theory for the self-rearrangement of embryonic cells and tissues. Journal of Biomechanical Engineering *124*, 188–197.

Campbell, K., and Casanova, J. (2016). A common framework for EMT and collective cell migration. Development *143*, 4291–4300. https://doi.org/10.1242/dev.139071.

Canty, L., Zarour, E., Kashkooli, L., François, P., and Fagotto, F. (2017). Sorting at embryonic boundaries requires high heterotypic interfacial tension. Nature Communications *8*, 157. https://doi.org/10.1038/s41467-017-00146-x.

Charras, G., and Sahai, E. (2014). Physical influences of the extracellular environment on cell migration. Nature Reviews. Molecular Cell Biology *15*, 813–824. https://doi.org/10.1038/nrm3897.

Charras, G., and Yap, A.S. (2018). Tensile Forces and Mechanotransduction at Cell-Cell Junctions. Current Biology: CB *28*, R445–R457. https://doi.org/10.1016/j.cub.2018.02.003.

Chaves-Pérez, A., MacK, B., Maetzel, D., Kremling, H., Eggert, C., Harréus, U., and Gires, O. (2013). EpCAM regulates cell cycle progression via control of cyclin D1 expression. Oncogene *32*, 641–650. https://doi.org/10.1038/onc.2012.75.

Cickovski, T.M., Huang, C., Chaturvedi, R., Glimm, T., Hentschel, H.G.E., Alber, M.S., Glazier, J.A., Newman, S.A., and Izaguirre, J.A. (2005). A framework for three-dimensional simulation of morphogenesis. IEEE/ACM Trans Comput Biol Bioinform *2*, 273–288. https://doi.org/10.1109/TCBB.2005.46.

Dai, X., Cheng, H., Bai, Z., and Li, J. (2017). J o u r n a l o f C a n c e r Breast Cancer Cell Line Classification and Its Relevance with Breast Tumor Subtyping. *8*. https://doi.org/10.7150/jca.18457.

Fagotto, F. (2020a). EpCAM as Modulator of Tissue Plasticity. Cells *9*, 2128. https://doi.org/10.3390/cells9092128.

Fagotto, F. (2020b). Cell sorting at embryonic boundaries. Seminars in Cell & Developmental Biology *107*, 126–129. https://doi.org/10.1016/j.semcdb.2020.07.012.

Fagotto, F. (2020c). Tissue segregation in the early vertebrate embryo. Seminars in Cell & Developmental Biology *107*, 130–146. https://doi.org/10.1016/j.semcdb.2020.05.020.

Fagotto, F., and Aslemarz, A. (2020). EpCAM cellular functions in adhesion and migration, and potential impact on invasion: A critical review. Biochimica et Biophysica Acta (BBA)-Reviews on Cancer *1874*, 188436.

Friedl, P., Locker, J., Sahai, E., and Segall, J.E. (2012). Classifying collective cancer cell invasion. Nat Cell Biol *14*, 777–783. https://doi.org/10.1038/ncb2548.

Gaber, A., Kim, S.J., Kaake, R.M., Benčina, M., Krogan, N., Šali, A., Pavšič, M., and Lenarčič, B. (2018). EpCAM homo-oligomerization is not the basis for its role in cell-cell adhesion. Scientific Reports *8*, 1–16. https://doi.org/10.1038/s41598-018-31482-7.

Gao, J., Yan, Q., Wang, J., Liu, S., and Yang, X. (2015). Epithelial-to-mesenchymal transition induced by TGF-beta1 is mediated by AP1-dependent EpCAM expression in MCF-7 cells. J Cell Physiol *230*, 775–782. https://doi.org/10.1002/jcp.24802.

Gaston, C., De Beco, S., Doss, B., Pan, M., Gauquelin, E., D'Alessandro, J., Lim, C.T., Ladoux, B., and Delacour, D. (2021). EpCAM promotes endosomal modulation of the cortical RhoA zone for epithelial organization. Nature Communications *12*, 1–22. https://doi.org/10.1038/s41467-021-22482-9.

Gires, O., and Bauerle, P.A. (2010). EpCAM as a target in cancer therapy. Journal of Clinical Oncology: Official Journal of the American Society of Clinical Oncology *28*, e239-40; author reply e241-2. https://doi.org/10.1200/JCO.2009.26.8540.

Glazier, J.A., and Graner, F. (1993). Simulation of the differential adhesion driven rearrangement of biological cells. Phys Rev E Stat Phys Plasmas Fluids Relat Interdiscip Topics *47*, 2128–2154.

Graner, F., and Glazier, J.A. (1992). Simulation of biological cell sorting using a two-dimensional extended Potts model. Phys. Rev. Lett. *69*, 2013–2016. https://doi.org/10.1103/PhysRevLett.69.2013.

Guerra, E., Lattanzio, R., la Sorda, R., Dini, F., Tiboni, G.M., Piantelli, M., and Alberti, S. (2012). mTrop1/Epcam Knockout Mice Develop Congenital Tufting Enteropathy through Dysregulation of Intestinal E-cadherin/β-catenin. PLoS ONE *7*. https://doi.org/10.1371/journal.pone.0049302.

Insua-Rodríguez, J., and Oskarsson, T. (2016). The extracellular matrix in breast cancer. Advanced Drug Delivery Reviews *97*, 41–55. https://doi.org/10.1016/j.addr.2015.12.017.

Izaguirre, J.A., Chaturvedi, R., Huang, C., Cickovski, T., Coffland, J., Thomas, G., Forgacs, G., Alber, M., Hentschel, G., Newman, S.A., et al. (2004). COMPUCELL, a multi-model framework for simulation of morphogenesis. Bioinformatics *20*, 1129–1137. https://doi.org/10.1093/bioinformatics/bth050.

Jolly, M.K., Mani, S.A., and Levine, H. (2018). Hybrid epithelial/mesenchymal phenotype(s): The "fittest" for metastasis? Biochim Biophys Acta Rev Cancer *1870*, 151–157. https://doi.org/10.1016/j.bbcan.2018.07.001.

Kashkooli, L., Rozema, D., Espejo-Ramirez, L., Lasko, P., and Fagotto, F. (2021). Ectoderm to mesoderm transition by down-regulation of actomyosin contractility. PLoS Biology *19*, e3001060. https://doi.org/10.1371/journal.pbio.3001060.

Koch, C., Kuske, A., Joosse, S.A., Yigit, G., Sflomos, G., Thaler, S., Smit, D.J., Werner, S., Borgmann, K., Gärtner, S., et al. (2020). Characterization of circulating breast cancer cells with tumorigenic and metastatic capacity. EMBO Molecular Medicine *12*, e11908. https://doi.org/10.15252/emmm.201911908.

Kramer, N., Walzl, A., Unger, C., Rosner, M., Krupitza, G., Hengstschläger, M., and Dolznig, H. (2013). In vitro cell migration and invasion assays. Mutation Research - Reviews in Mutation Research *752*, 10–24. https://doi.org/10.1016/j.mrrev.2012.08.001.

Kuhn, S., Koch, M., Nu, T., Ladwein, M., Antolovic, D., Klingbeil, P., Hildebrand, D., Moldenhauer, G., Langbein, L., Franke, W.W., et al. (2007). A Complex of EpCAM, Claudin-7, CD44 Variant Isoforms, and Tetraspanins Promotes Colorectal Cancer Progression. *5*, 553–568. https://doi.org/10.1158/1541-7786.MCR-06-0384.

Leckband, D.E., and de Rooij, J. (2014). Cadherin adhesion and mechanotransduction. Annual Review of Cell and Developmental Biology *30*, 291–315. https://doi.org/10.1146/annurev-cellbio-100913-013212.

Lecuit, T., and Lenne, P.F. (2007). Cell surface mechanics and the control of cell shape, tissue patterns and morphogenesis. Nat Rev Mol Cell Biol *8*, 633–644. https://doi.org/10.1038/nrm2222.

Lei, Z., Maeda, T., Tamura, A., Nakamura, T., Yamazaki, Y., Shiratori, H., Yashiro, K., Tsukita, S., and Hamada, H. (2012). EpCAM contributes to formation of functional tight junction in the intestinal epithelium by recruiting claudin proteins. Developmental Biology *371*, 136–145. https://doi.org/10.1016/j.ydbio.2012.07.005.

Lenárt, S., Lenárt, P., Šmarda, J., Remšík, J., Souček, K., and Beneš, P. (2020). Trop2: Jack of All Trades, Master of None. Cancers *12*. https://doi.org/10.3390/cancers12113328.

Litvinov, S.V., Bakker, H.A., Gourevitch, M.M., Velders, M.P., and Warnaar, S.O. (1994). Evidence for a role of the epithelial glycoprotein 40 (Ep-CAM) in epithelial cell-cell adhesion. Cell Adhes Commun *2*, 417–428. https://doi.org/10.3109/15419069409004452.

Maetzel, D., Denzel, S., Mack, B., Canis, M., Went, P., Benk, M., Kieu, C., Papior, P., Baeuerle, P.A., Munz, M., et al. (2009). Nuclear signalling by tumour-associated antigen EpCAM. Nature Cell Biology *11*, 162–171. https://doi.org/10.1038/ncb1824.

Maghzal, N., Vogt, E., Reintsch, W., Fraser, J.S., and Fagotto, F. (2010). The tumor-associated EpCAM regulates morphogenetic movements through intracellular signaling. Journal of Cell Biology *191*, 645–659. https://doi.org/10.1083/jcb.201004074.

Maghzal, N., Kayali, H.A., Rohani, N., Kajava, A. V., and Fagotto, F. (2013). EpCAM Controls Actomyosin Contractility and Cell Adhesion by Direct Inhibition of PKC. Developmental Cell *27*, 263–277. https://doi.org/10.1016/j.devcel.2013.10.003.

Mayor, R., and Etienne-Manneville, S. (2016). The front and rear of collective cell migration. Nature Reviews. Molecular Cell Biology *17*, 97–109. https://doi.org/10.1038/nrm.2015.14.

Milloud, R., Destaing, O., de Mets, R., Bourrin-Reynard, I., Oddou, C., Delon, A., Wang, I., Albigès-Rizo, C., and Balland, M. (2017). αvβ3 integrins negatively regulate cellular forces by phosphorylation of its distal NPXY site. Biology of the Cell *109*, 127–137. https://doi.org/10.1111/boc.201600041.

Nakato, G., Morimura, S., Lu, M., Feng, X., Wu, C., and Udey, M.C. (2020). Amelioration of Congenital Tufting Enteropathy in EpCAM (TROP1)-Deficient Mice via Heterotopic Expression of TROP2 in Intestinal Epithelial Cells. Cells *9*. https://doi.org/10.3390/cells9081847.

Nubel, T., Preobraschenski, J., Tuncay, H., Weiss, T., Kuhn, S., Ladwein, M., Langbein, L., and Zoller, M. (2009). Claudin-7 regulates EpCAM-mediated functions in tumor progression. Mol Cancer Res *7*, 285–299. https://doi.org/10.1158/1541-7786.MCR-08-0200.

Osta W.A., Chen Y., Mikhitarian K., Mitas M., Salem M., Hannun Y.A., Cole D.J., Gillanders W.E. (2004). EpCAM is overexpressed in breast cancer and is a potential target for breast cancer gene therapy, Cancer Res. *64*, 5818–5824.

[96] M. Trebak, G.E. Begg, J.M. Chong, E.V. Kanazireva, D. Herlyn, D.W. Speicher,Pan, M., Schinke, H., Luxenburger, E., Kranz, G., Shakhtour, J., Libl, D., Huang, Y., Gaber, A., Pavšič, M., Lenarčič, B., et al. (2018). EpCAM ectodomain EpEX is a ligand of EGFR that counteracts EGF-mediated epithelial-mesenchymal transition through modulation of phospho-ERK1/2 in head and neck cancers.

Parent, S.E., Barua, D., and Winklbauer, R. (2017). Mechanics of Fluid-Filled Interstitial Gaps. I. Modeling Gaps in a Compact Tissue. Biophysical Journal *113*, 913–922. https://doi.org/10.1016/j.bpj.2017.06.062.

Rao, C.G., Chianese, D., Doyle, G. V., Miller, M.C., Russell, T., Sanders, R.A., and Terstappen, L.W.M.M. (2005). Expression of epithelial cell adhesion molecule in carcinoma cells present in blood and primary and metastatic tumors. International Journal of Oncology *27*, 49–57. https://doi.org/10.3892/ijo.27.1.49.

Rohani, N., Parmeggiani, A., Winklbauer, R., and Fagotto, F. (2014). Variable combinations of specific ephrin ligand/Eph receptor pairs control embryonic tissue separation. PLoS Biology *12*, e1001955. https://doi.org/10.1371/journal.pbio.1001955.

Sabass, B., Gardel, M.L., Waterman, C.M., and Schwarz, U.S. (2008). High resolution traction force microscopy based on experimental and computational advances. Biophysical Journal *94*, 207–220. https://doi.org/10.1529/biophysj.107.113670.

Salomon, J., Gaston, C., Magescas, J., Duvauchelle, B., Canioni, D., Sengmanivong, L., Mayeux, A., Michaux, G., Campeotto, F., Lemale, J., et al. (2017). Contractile forces at tricellular contacts modulate epithelial organization and monolayer integrity. Nature Communications *8*. https://doi.org/10.1038/ncomms13998.

Sankpal, N. V., Mayfield, J.D., Willman, M.W., Fleming, T.P., and Gillanders, W.E. (2011). Activator protein 1 (AP-1) contributes to EpCAM-dependent breast cancer invasion. Breast Cancer Research *13*, 1–13. https://doi.org/10.1186/bcr3070.

Sankpal, N. V., Fleming, T.P., Sharma, P.K., Wiedner, H.J., and Gillanders, W.E. (2017). A double-negative feedback loop between EpCAM and ERK contributes to the regulation of

epithelial-mesenchymal transition in cancer. Oncogene *36*, 3706–3717. https://doi.org/10.1038/onc.2016.504.

Sivagnanam, M., Mueller, J.L., Lee, H., Chen, Z., Nelson, S.F., Turner, D., Zlotkin, S.H., Pencharz, P.B., Ngan, B.Y., Libiger, O., et al. (2008). Identification of EpCAM as the Gene for Congenital Tufting Enteropathy. Gastroenterology *135*, 429–437. https://doi.org/10.1053/j.gastro.2008.05.036.

Slanchev, K., Carney, T.J., Stemmler, M.P., Koschorz, B., Amsterdam, A., Schwarz, H., and Hammerschmidt, M. (2009). The epithelial cell adhesion molecule EpCAM is required for epithelial morphogenesis and integrity during zebrafish epiboly and skin development. PLoS Genetics *5*. https://doi.org/10.1371/journal.pgen.1000563.

Švec, J., Šťastná, M., Janečková, L., Hrčkulák, D., Vojtěchová, M., Onhajzer, J., Kříž, V., Galušková, K., Šloncová, E., Kubovčiak, J., et al. (2022). TROP2 Represents a Negative Prognostic Factor in Colorectal Adenocarcinoma and Its Expression Is Associated with Features of Epithelial-Mesenchymal Transition and Invasiveness. Cancers (Basel) *14*, 4137. https://doi.org/10.3390/cancers14174137.

Tse, J.R., and Engler, A.J. (2010). Preparation of hydrogel substrates with tunable mechanical properties. Current Protocols in Cell Biology 1–16. https://doi.org/10.1002/0471143030.cb1016s47.

Tseng, Q., Duchemin-Pelletier, E., Deshiere, A., Balland, M., Guilloud, H., Filhol, O., and Théry, M. (2012). Spatial organization of the extracellular matrix regulates cell-cell junction positioning. Proceedings of the National Academy of Sciences of the United States of America *109*, 1506–1511. https://doi.org/10.1073/pnas.1106377109.

Vannier, C., Mock, K., Brabletz, T., and Driever, W. (2013). Zeb1 regulates E-cadherin and Epcam (epithelial cell adhesion molecule) expression to control cell behavior in early zebrafish development. Journal of Biological Chemistry *288*, 18643–18659. https://doi.org/10.1074/jbc.M113.467787.

Vignaud, T., Ennomani, H., and Théry, M. (2014). Polyacrylamide Hydrogel Micropatterning. Methods in Cell Biology *120*, 93–116. https://doi.org/10.1016/B978-0-12-417136-7.00006-9.

Wang, J., Zhang, K., Grabowska, D., Li, A., Dong, Y., Day, R., Humphrey, P., Lewis, J., Kladney, R.D., Arbeit, J.M., et al. (2011). Loss of Trop2 promotes carcinogenesis and features of epithelial to mesenchymal transition in squamous cell carcinoma. Molecular Cancer Research *9*, 1686–1695. https://doi.org/10.1158/1541-7786.MCR-11-0241.

Wang, M.H., Sun, R., Zhou, X.M., Zhang, M.Y., Lu, J. Bin, Yang, Y., Zeng, L.S., Yang, X.Z., Shi, L., Xiao, R.W., et al. (2018). Epithelial cell adhesion molecule overexpression regulates epithelial-mesenchymal transition, stemness and metastasis of nasopharyngeal carcinoma cells via the PTEN/AKT/mTOR pathway. Cell Death and Disease *9*. https://doi.org/10.1038/s41419-017-0013-8.

Went, P.T., Lugli, A., Meier, S., Bundi, M., Mirlacher, M., Sauter, G., and Dirnhofer, S. (2004). Frequent EpCam Protein Expression in Human Carcinomas. Human Pathology *35*, 122–128. https://doi.org/10.1016/j.humpath.2003.08.026.

Winklbauer, R. (2015). Cell adhesion strength from cortical tension – an integration of concepts. *2*, 3687–3693. https://doi.org/10.1242/jcs.174623.

Wu, C.J., Lu, M., Feng, X., Nakato, G., and Udey, M.C. (2020). Matriptase Cleaves EpCAM and TROP2 in Keratinocytes, Destabilizing Both Proteins and Associated Claudins. Cells *9*. https://doi.org/10.3390/cells9041027.

Figure legends

Figure 1. Cohesive collective migration of MCF7 spheroids is stimulated by EpCAM KD, but inhibited by Trop2 KD.

Spheroids of transfected MCF7 cells with control, EpCAM, Trop2 and EpCAM/Trop2 siRNA were plated on a layer of fibrillar collagen gel, let adhere for 30 minutes, then phase contrast images were taken every 30min for 24hrs. **A-D.** Images of whole spheroids at selected time points. Scale bar = 100µm. **E.** Quantification of relative area increase after 24hrs, expressed as ratio of the final and initial areas. 45-63 spheroids from six to nine independent experiments, combining four experiments with siTrop2 sc-43043 and two with siTrop2 H502-0033, see supplemental Fig.S1E for separate results. In all figures, the box plots show the interquartile range (box limits), median (center line), and min and max values without outliers (whiskers). Statistical analysis: One-way non-parametric ANOVA (Kruskal-Wallis Test) followed by Dunn post hoc test. For all experiments presented in this study, P values are indicated as follows: * $P < 0.05$, ** $P < 0.01$, *** $P < 0.001$ and NS, not significant. **F.** Quantification of spheroids solidity, measured as the ratio [Area]/[Area of convex hull]. Quantification from the six experiments. **G.** Schematic representation of typical spheroid morphologies in top and orthogonal views. **H, H'.** Examples of phalloidin-labelled spheroids after 24hrs spreading in top and orthogonal view. **H".** Details of spheroid edges. Maximal projection of 3 z planes, 1µm apart. Protrusions are observed in all conditions (arrowheads). However, control and Trop2 KD spheroids have numerous cells protruding out of the main cell mass (asterisks), which are rare in EpCAM KD and dKD. These are rather characterized by frequent actin cable-like structures along the spheroid edge (arrows).

Figure 2. The effect EpCAM KD on spheroid collective migration is dependent on PKC and myosin II activity, and is accompanied by pMLC and E-cadherin upregulation.

A. Scheme representing EpCAM negative regulation of the nPKC - myosin II pathway with the corresponding chemical inhibitors calphostin and blebbistatin. **B.** Myosin II and nPKC inhibition rescue the EpCAM KD spreading phenotype in a dose-dependent manner, and decrease spreading of wild type spheroids. Spreading of control and EpCAM KD spheroids was tested in the absence or presence of 0.25 and 0.5µM calphostin C (Calph), or 2 and 5µM blebbistatin (Bleb). Area increase was normalized to untreated controls. 7-32 spheroids from 2-8 independent experiments. Statistical analysis: one-way ANOVA followed by Tukey-HSD post hoc test. **C-F.** E-cadherin and pMLC levels are elevated upon both EpCAM and Trop2 KD. **C,D.** Representative confocal images of spheroids after 24hrs spreading, immunolabelled for p-MLC and E-cadherin. Levels are visualized using the "fire" pseudocolors of ImageJ. The selected z planes correspond to the widest

area for each spheroid. Scale bar = 50μm. **E-G.** Quantification of p-MLC (E) and E-cadherin (F) mean intensities along cell outlines, and calculated E-cadherin/pMLC ratio (G). Both EpCAM and Trop2 KD cause an increase in both pMLC and E-cadherin. However, the E-cadherin to pMLC ratio is highest in EpCAM KD but lowest in Trop2 KD. Eight spheroids of each condition from three independent experiments. One-way non-parametric ANOVA (Kruskal-Wallis) followed by Dunn post hoc test.

Figure 3. Differential effect of EpCAM and Trop2 KD on myosin balance between cell contacts and free cortex, on E-cadherin levels, and on focal adhesions. A. Representative confocal images of small groups of cells immunolabelled for E-cadherin (red) and pMLC (green), with F-actin filaments labelled phalloidin-Alexa647 (magenta). **B-G.** Quantification of peak intensities, determined through complete z stack series, for p-MLC along free cell edges (B) and cell-cell contacts (C), E-cadherin at contacts (D), calculated ratios contact to edge for pMLC (E), and pMLC/E-cadherin for contacts (F). pMLC intensities were normalized to the median value of peak pMLC at edges of control cells. E-cadherin signal was normalized to control contacts. **G.** Confocal images of the ventral side of single cells on collagen gel, immunolabelled for vinculin. **H.** Quantification of total vinculin focal adhesion intensity, normalized relative to the median value of control cells. H' presents the vinculin signal divided by the cell area. Data from seven independent experiments (~80-180 cells/condition) for pMLC, E-cadherin and phalloidin (B-G), and from six experiments (~80 cells/condition) for vinculin (I). One-way non-parametric ANOVA (Kruskal-Wallis Test) followed by Dunn post-hoc test. Scale bars = 10 μm.

Figure 4. EpCAM KD and Trop2 KD differentially increase traction on the substrate, cortical tension and cell-cell adhesion. A-D. Traction Force Microscopy (TFM) of cell doublets on H patterns. **A.** Scheme of the experimental settings. Cells doublets were laid on H patterns coated with a thin layer of collagen (green) on a polyacrylamide gel with a stiffness of 5kPa, containing far red fluorescence nanobeads. Cells and underneath nanobeads were imaged, then cells were removed by trypsinization, and second images of the same positions were taken and used as reference, from which bead displacement was measured. **A'.** Diagram of force vectors obtained by TFM on H-shape micropatterns. While traction forces (black arrows) are measured from the displacement of nanobeads, the cell-cell force (red arrow) is calculated indirectly based on it counterbalancing the sum of traction forces, as shown in the equation. **B.** Representative images of micropattern-confined cell doublets for the four experimental conditions. **C.** Corresponding average maps of traction forces. **D.** Quantification of traction forces. **E.** Quantification of cell-cell

forces. **F.** Cell-cell force to traction force ratio. **G.** Quantification of junction lengths, measured from the phase contrast images. One-way ANOVA followed by Tukey-HSD post-hoc test.

H-L. Determination of relative cortical tension and cell-cell adhesiveness of cell doublets laid on a non-adhering surface. H. Diagram of an asymmetric cell doublet, with the balance between cortical tensions at the free edges ($\gamma_{m(A)}$ and $\gamma_{m(B)}$) and contact tension ($\gamma_{c(AB)}$). The principles of such system are as follows: The directions of $\gamma_{m(A)}$, $\gamma_{m(A)}$ and $\gamma_{c(AB)}$ are tangential to the membranes at the cell vertex, which allows to directly calculate the relative strengths of these tensions based on the geometry at vertices. The orange layer represents the actomyosin cortex, with its thickness symbolizing relative contractility. In the configuration represented in the diagram, the curved cell-cell interface reflects differences in cortical tension, as cell A tends to partly engulf B, due to its lower tension ($\gamma_{m(A)} < \gamma_{m(B)}$). The strength of adhesion is related to the capacity of downregulating cortical tension along the cell-cell contact ($2 * \gamma_{c(AB)} < \gamma_{m(A)} + \gamma_{m(B)}$). θ is the angle formed by the two vectors $\gamma_{m(A)}$ and $\gamma_{m(B)}$. It directly relates to adhesiveness, a dimensionless value that ranges from 0 to 1. **I,J.** Examples of homotypic and heterotypic doublets imaged by live confocal microscopy. The doublets were formed by mixing dissociated cells and let them re-associate on an adhesion-free support. Membranes were labeled with CellMask Alexa Fluor 647. siCtrl (A) cells were marked by Hoechst staining (showed in red) prior dissociation. Scale bar = 10μm. **K.** Quantification of relative cortical tensions expressed as the ratio $\gamma_{m(A)}/\gamma_{m(B)}$. As expected, under all conditions, the ratio is close to 1 for homotypic doublets. The ratio for heterotypic doublets is significantly lower, demonstrating that single and double depletions all cause an increase in cortical tension. **L.** Quantification of adhesiveness, calculated from γ_c and γ_m. Values for homotypic doublets show that doublets of EpCAM KD or dKD cells have increased adhesiveness compared to control cells. Trop2 KD only leads to a weak, non-significant increase. In the case of heterotypic doublets, however, adhesiveness appears decreased in all cases. Four independent experiments, total 500-1250 doublets. Experiment medians indicated by dots. One-way non-parametric ANOVA (Kruskal-Wallis Test) followed by Dunn post-hoc test.

Figure 5. Simulation of spheroid spreading in controls and under EpCAM/Trop2-depleted conditions based on biophysical parameters. A. Representation of schematic cell doublets on a substrate, with the relative tensions represented at the cell-cell vertex and at the edge of the matrix substrate interface. Their relative strength is represented by the length of the vector. The general changes in tensions between control and EpCAM KD, and between EpCAM KD and Trop2 KD are summarized in the two boxes with blue borders. **B**. Balance of forces at the cell-cell vertex. While all three tensions are strongly increased both in EpCAM KD and Trop2 KD, the resulting

adhesiveness, which can be directly deduced from the angle θ, is increased in EpCAM KD but not in Trop2 KD. **C**. Balance of forces at the matrix interface. γ_s is the tension exerted on the substrate, corresponding to the traction measured by TFM. It counterbalances the cell-matrix tension γ_x and the horizontal component of the cell-medium tension γ_m. Both tensions are increased in EpCAM and Trop2 KD, but their relative balance determines different outcomes: EpCAM KD cells adopts a spread configuration (acute angle ϕ), while, on the contrary, Trop2 KD cells have a compact shape (obtuse angle ϕ).

D-F. Simulation of spheroids spreading using a 3D cellular Potts model (CompuCell3D software) for control, EpCAM KD and Trop2 KD conditions. See annex for detailed information. Images correspond to examples of yx and yz planes after 300 iterations. Medium is in light blue, matrix substrate in dark blue. **D'-D'.** Outlines of explants at 24hrs from Fig.1, drawn for comparison. **G.** Energy parameters used to simulate the three conditions. **H,H'.** Comparison of curves of relative area expansion from experimental data and from simulation. Error bars: SD.

Figure 6. Differences in EpCAM and Trop2 distribution along the plasma membrane account for the distinct phenotypes. **A. Localization in wild type cells.** Confocal microscopy image of groups of wild-type MCF cells on collagen gel, labelled under non-permeabilized conditions for EpCAM (green), Trop2 (red) and F-actin (phalloidin-Alexa647, magenta). EpCAM and Trop2 levels where analyzed from whole z-stacks, as well from resliced stacks to obtain z projections (see details in suppl. Fig.S6). Both EpCAM and Trop2 were found distributed all along the membrane. **A.** Merged image. **A',A",A'''.** Individual channels. **A''''**. Maximal projection of the whole stack. **B.** Example of z projection. The position of the slice is indicated by the white dashed line in A. EpCAM and Trop2 channels are displayed as "fire" pseudocolours. The patterns of the two regulators appear virtually identical, except for slightly higher Trop2 levels at the ventral side (yellow arrowheads). **C-F. Quantification of relative levels of EpCAM and Trop2. C.** Levels in three regions of control embryos, indicated in the diagram C', and reciprocal impact of EpCAM and Trop2 depletions. A larger set of 12 categories was quantified, see suppl. Fig.S6 for full analysis. All values were normalized to the average intensity for EpCAM or for Trop2 at cell contacts of control cells (contact ave, see suppl. Fig.S6A). In control groups, cell contacts and dorsal side had similar relative levels of EpCAM and Trop2. The ventral side showed the lowest levels, but a relative enrichment in Trop2 versus EpCAM was reproducibly observed. Trop2 KD had no significant impact on EpCAM levels and distribution. EpCAM KD led to a decrease of Trop2 at contacts and dorsal side (and most locations, suppl. Fig.S6C), but a significant enrichment on the ventral side. **D.** Direct pairwise comparison of dorsal to ventral ratios for EpCAM and Trop2 in

wild type cell groups. The ratio is significantly lower for Trop2. **E,F.** Effect of Trop2 and EpCAM depletions on the dorsal-ventral ratio (E) and on the ratio dorsal side versus average cell contact (F). EpCAM is not significantly affected by Trop2 KD, but Trop2 ratios are strongly decreased in EpCAM KD. All quantifications were on 13-15 groups of cells (4-8 cells per group) from three independent experiments. Statistical analysis: C: Non-parametric ANOVA (Kruskal-Wallis Test) followed by post-hoc Pairwise Mann-Whitney tests. D-F: Student's t-test.

G. Summary diagram of EpCAM and Trop2 cell surface distribution in wild type cells and changes occurring upon EpCAM or Trop2 KD. Relative levels are symbolized by red and green colour scales. Depletion is symbolized by grey cells. Blue arrows of different sizes point to Trop2 levels and changes observed upon EpCAM KD. The result is a relative enrichment at the ventral and cell contact sites relative to dorsal. This change is compatible with a decrease in corresponding tension balances, stimulating spreading on the substrate and cell-cell adhesion. Purple arrows point to the absence of significant changes for EpCAM levels in Trop2 KD, indicating that the Trop2 KD phenotype is mainly due to the decrease of the Trop2-dependent regulation. In particular, lower spreading can be explained by the loss of the ventral Trop2 pool, leading to relatively higher contractility compared to the dorsal side.

Figure 7. EpCAM depletion prevents single cell escape

A-D. Selected time frames of time lapse movies showing edges of spheroids. Control MCF7 spheroids occasionally show single cells breaking off and migrating away (A, arrow). This never happens, at least within 24hrs of imaging, for siEpCAM spheroids (B), while it does occur in siTrop2 (C). **E.** Proportion of spheroids showing at least one cell or one cell group migrating away during 24hrs. Data from 84, 85, 51 and 50 spheroids (corresponding to siCtrl, siEpCAM, siTrop2 and dKD respectively) from 12 independent experiments. Statistical analysis: Non-parametric ANOVA (Kruskal-Wallis Test) followed by post-hoc Dunn tests.

Supplemental material

Annex. Description of simulation (cellular Potts model).

Figure S1. Related to Fig.1.

Figure S2. Related to Fig.1.

Figure S3. Related to Figs.1,4,5.

Figure S4. Related to Fig.3.

Figure S5. Related to Figs.4 and 7.

Figure S6. Related to Fig.6.

Figure S7. Related to Figs.7.

Movie 1. Related to Figure 1A.
Time lapse of spreading of siCtrl spheroid on fibrillar collagen.

Movie 2. Related to Figure 1A.
Time lapse of spreading of siEpCAM spheroid on fibrillar collagen.

Movie 3. Related to Figure 1A.
Time lapse of spreading of siTrop2 spheroid on fibrillar collagen.

Movie 4. Related to Figure 1A.
Time lapse of spreading of dKD spheroid on fibrillar collagen.

Movie 5. Related to supplemental Figure S3A.
Time lapse of migration of single siCtrl cell on fibrillar collagen.

Movie 6. Related to supplemental Figure S3A.
Time lapse of migration of single siEpCAM cell on fibrillar collagen.

Movie 7. Related to supplemental Figure S3A.
Time lapse of migration of single siTrop2 cell on fibrillar collagen.

Movie 8. Related to supplemental Figure S3A.
Time lapse of migration of single dKD cell on fibrillar collagen.

Movie 9. Related to Figure 5.
Time lapse of simulation of spheroid spreading on the matrix substrate (blue) using 3D Cellular Potts Model. 3D view.

Movie 10. Related to Figure 5.
Simulation of spheroid spreading on the matrix substrate. Top: xz projection. Bottom: xy projection, plane closest to the substrate.

Movie 11. Related to supplemental Figure 7.
Partial view of control spheroid spreading with detachment of a single cell.

Movie 12. Related to supplemental Figure 7.
Partial view of siEpCAM spheroid spreading, without cell detachment.

Movie 13. Related to supplemental Figure 7.
Partial view of siTrop2 spheroid spreading with detachment of a pair of cells.

Movie 14. Related to supplemental Figure 7.
Partial view of dKD spheroid spreading, without cell detachment.

Figure 1

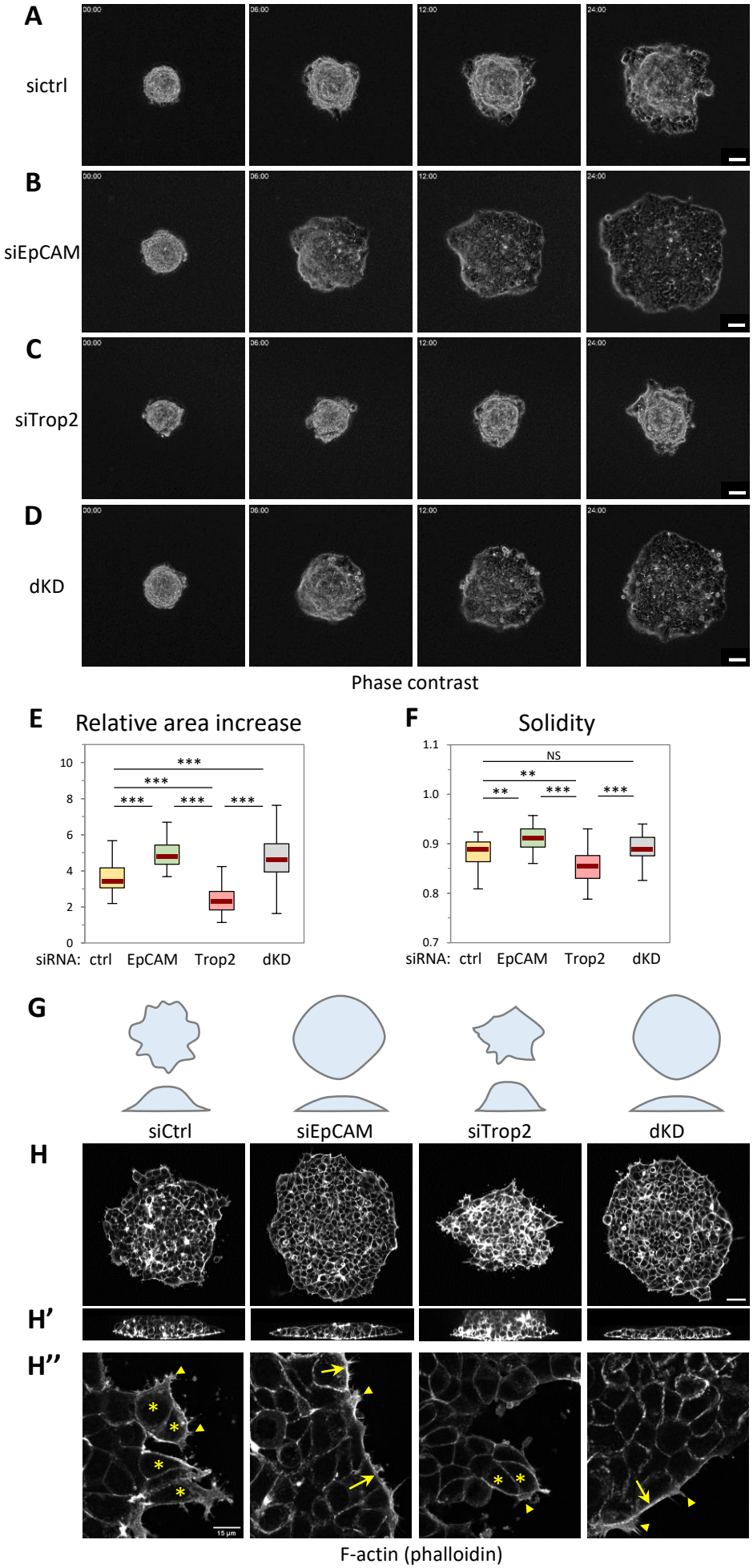
A
sictrl
B
siEpCAM
C
siTrop2
D
dKD
00:00
06:00
12:00
24:00
Phase contrast
E
Relative area increase
10
8
6
4
2
0
***
siRNA: ctrl EpCAM Trop2 dKD
F
Solidity
1.1
1.0
0.9
0.8
0.7
NS
**
siRNA: ctrl EpCAM Trop2 dKD
G
siCtrl
siEpCAM
siTrop2
dKD
H
H'
H''
15 µm
F-actin (phalloidin)

Figure 2

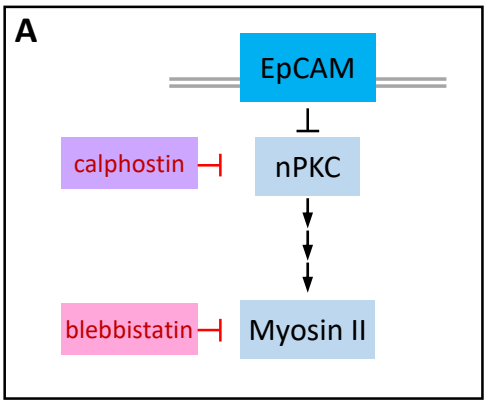
A
EpCAM
calphostin
nPKC
blebbistatin
Myosin II

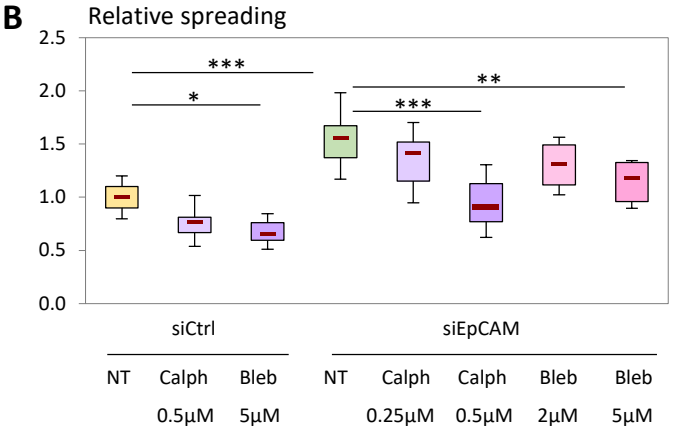
B
Relative spreading
2.5
2.0
1.5
1.0
0.5
0.0
***
*
***
**
siCtrl
siEpCAM
NT
Calph 0.5µM
Bleb 5µM
NT
Calph 0.25µM
Calph 0.5µM
Bleb 2µM
Bleb 5µM

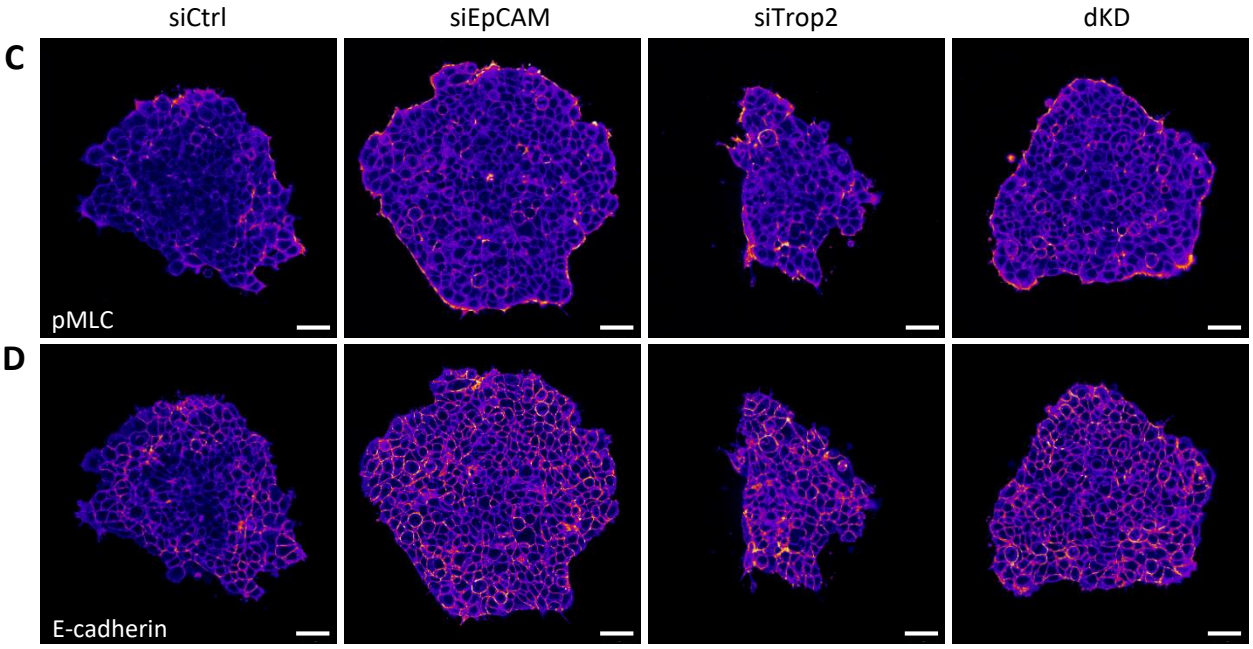
siCtrl
siEpCAM
siTrop2
dKD
C
pMLC
D
E-cadherin

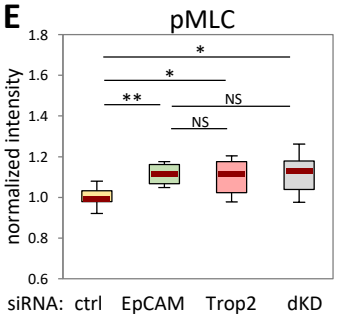
E
pMLC
normalized intensity
1.8
1.6
1.4
1.2
1.0
0.8
0.6
*
*
**
NS
NS
siRNA: ctrl
EpCAM
Trop2
dKD

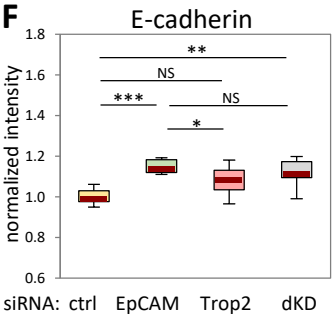
F
E-cadherin
normalized intensity
1.8
1.6
1.4
1.2
1.0
0.8
0.6
**
NS
***
NS
*
siRNA: ctrl
EpCAM
Trop2
dKD

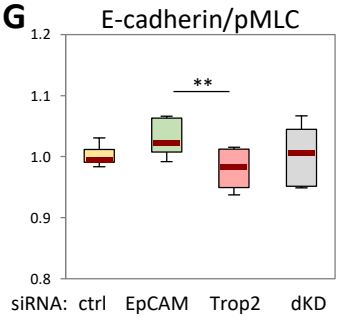
G
E-cadherin/pMLC
1.2
1.1
1.0
0.9
0.8
**
siRNA: ctrl
EpCAM
Trop2
dKD

Figure 3

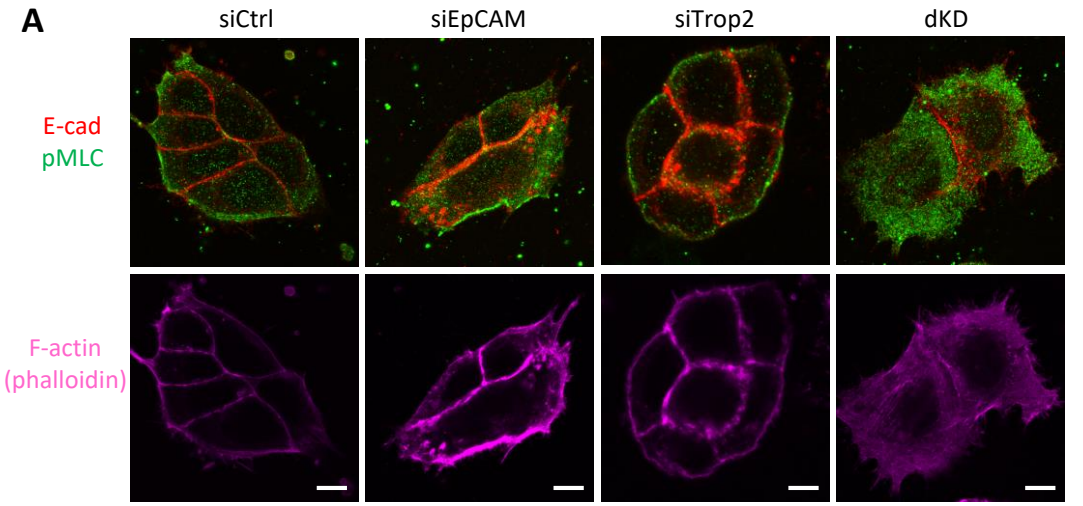
A
siCtrl
siEpCAM
siTrop2
dKD
E-cad
pMLC
F-actin
(phalloidin)

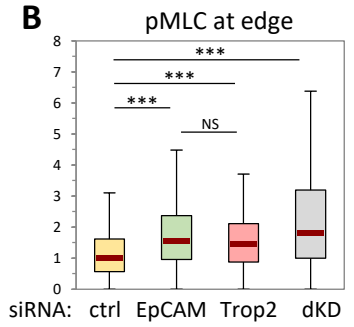
B
pMLC at edge
***
***
***
NS
siRNA: ctrl EpCAM Trop2 dKD

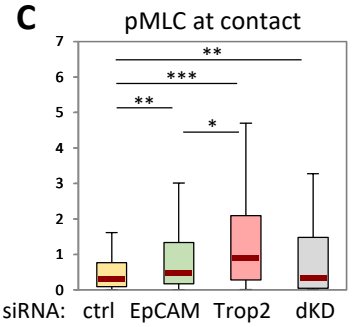
C
pMLC at contact
**
***
**
*
siRNA: ctrl EpCAM Trop2 dKD

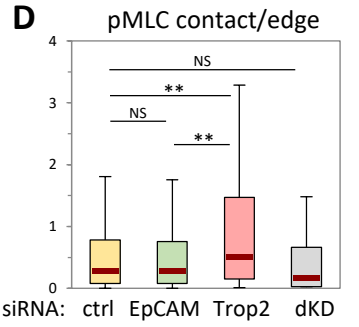
D
pMLC contact/edge
NS
**
NS
**
siRNA: ctrl EpCAM Trop2 dKD

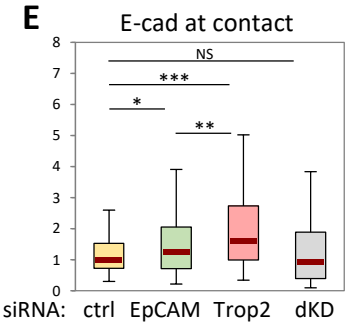
E
E-cad at contact
NS
***
*
**
siRNA: ctrl EpCAM Trop2 dKD

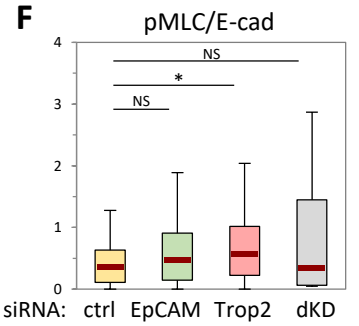
F
pMLC/E-cad
NS
*
NS
siRNA: ctrl EpCAM Trop2 dKD

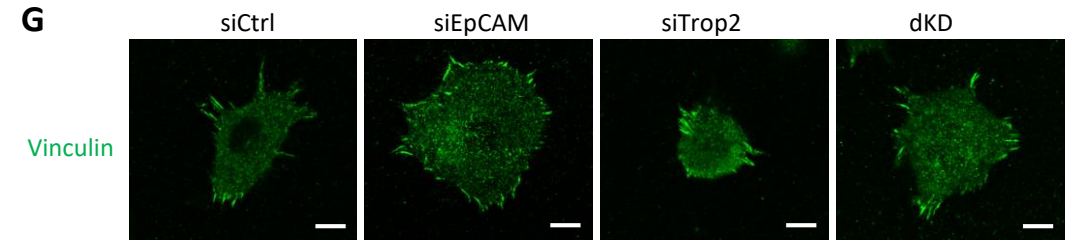
G
siCtrl
siEpCAM
siTrop2
dKD
Vinculin

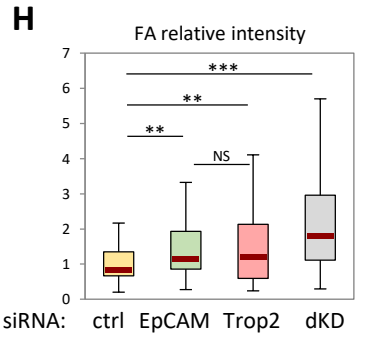
H
FA relative intensity
***
**
**
NS
siRNA: ctrl EpCAM Trop2 dKD

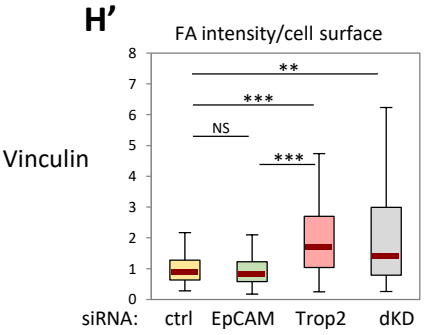
H'
FA intensity/cell surface
Vinculin
**
***
NS
***
siRNA: ctrl EpCAM Trop2 dKD

Figure 4

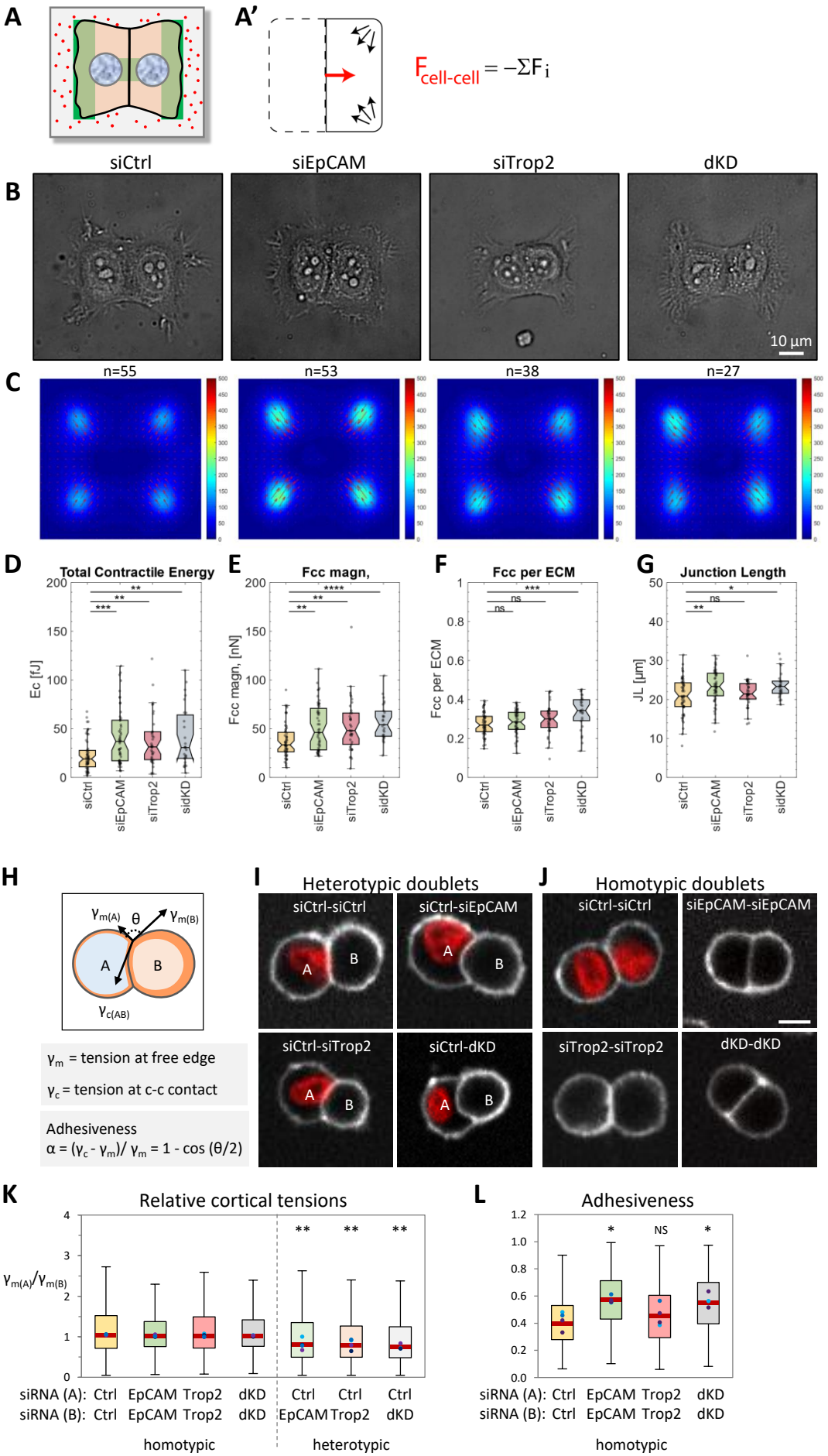
A
A'
$F_{cell-cell} = -\Sigma F_i$
B
siCtrl
siEpCAM
siTrop2
dKD
10 µm
C
n=55
n=53
n=38
n=27
D
Total Contractile Energy
Ec [fJ]
E
Fcc magn,
Fcc magn, [nN]
F
Fcc per ECM
Fcc per ECM
G
Junction Length
JL [µm]
siCtrl
siEpCAM
siTrop2
sidKD
H
$\gamma_{m(A)}$
θ
$\gamma_{m(B)}$
A
B
$\gamma_{c(AB)}$
γ_m = tension at free edge
γ_c = tension at c-c contact
Adhesiveness
$\alpha = (\gamma_c - \gamma_m)/\gamma_m = 1 - \cos(\theta/2)$
I
Heterotypic doublets
siCtrl-siCtrl
siCtrl-siEpCAM
siCtrl-siTrop2
siCtrl-dKD
J
Homotypic doublets
siCtrl-siCtrl
siEpCAM-siEpCAM
siTrop2-siTrop2
dKD-dKD
K
Relative cortical tensions
$\gamma_{m(A)}/\gamma_{m(B)}$
siRNA (A): Ctrl EpCAM Trop2 dKD Ctrl Ctrl Ctrl
siRNA (B): Ctrl EpCAM Trop2 dKD EpCAM Trop2 dKD
homotypic
heterotypic
L
Adhesiveness
NS
siRNA (A): Ctrl EpCAM Trop2 dKD
siRNA (B): Ctrl EpCAM Trop2 dKD
homotypic

Figure 5

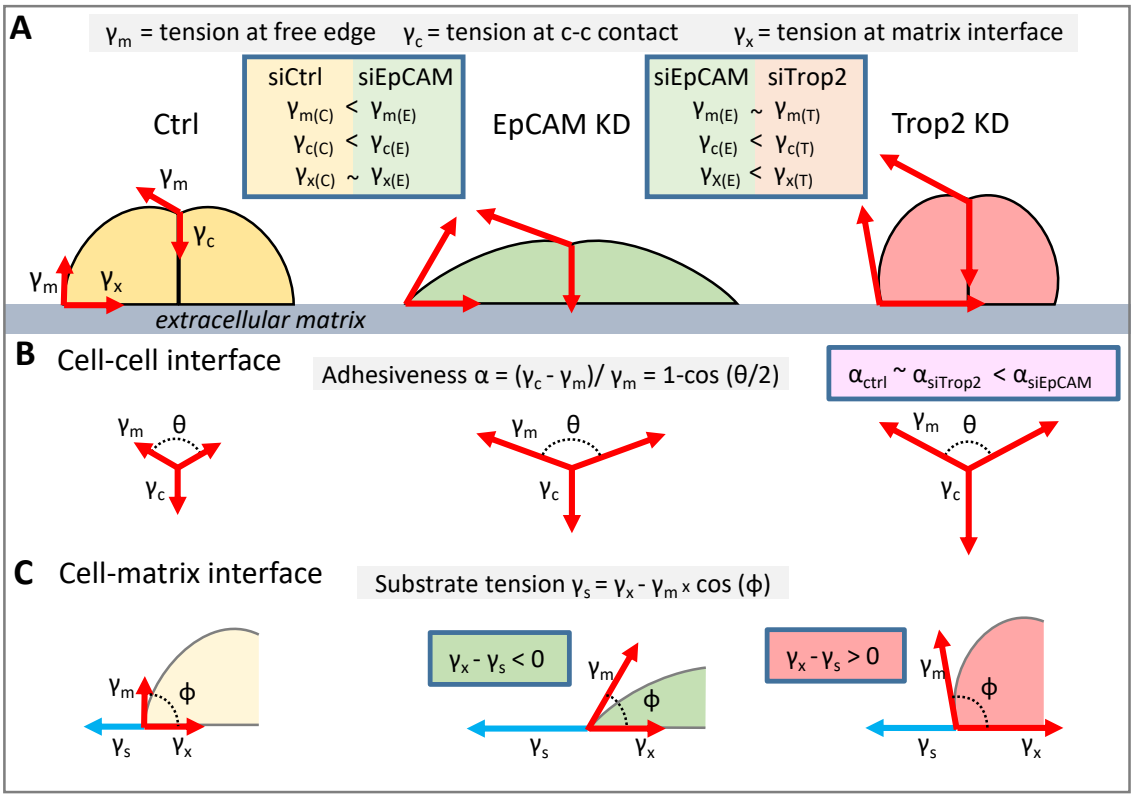
A
γm = tension at free edge
γc = tension at c-c contact
γx = tension at matrix interface
Ctrl
siCtrl siEpCAM
γm(C) < γm(E)
γc(C) < γc(E)
γx(C) ~ γx(E)
EpCAM KD
siEpCAM siTrop2
γm(E) ~ γm(T)
γc(E) < γc(T)
γX(E) < γx(T)
Trop2 KD
extracellular matrix
B Cell-cell interface
Adhesiveness α = (γc - γm)/ γm = 1-cos (θ/2)
αctrl ~ αsiTrop2 < αsiEpCAM
C Cell-matrix interface
Substrate tension γs = γx - γm x cos (ϕ)
γx - γs < 0
γx - γs > 0

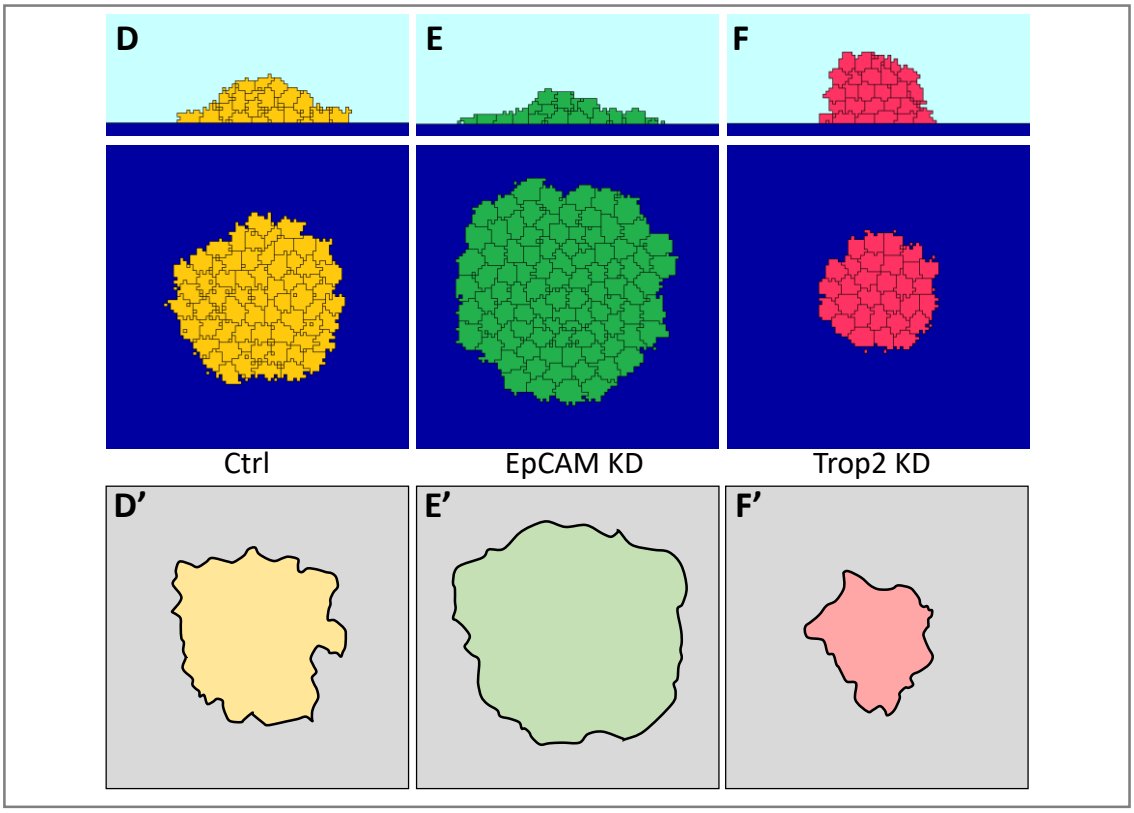
D
E
F
Ctrl
EpCAM KD
Trop2 KD
D'
E'
F'

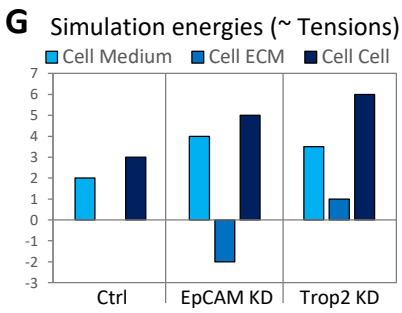
G Simulation energies (~ Tensions)
Cell Medium
Cell ECM
Cell Cell
Ctrl
EpCAM KD
Trop2 KD

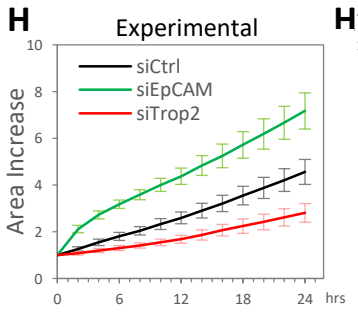
H Experimental
Area Increase
siCtrl
siEpCAM
siTrop2
hrs

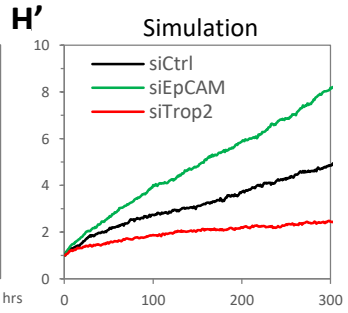
H' Simulation
siCtrl
siEpCAM
siTrop2

Figure 6

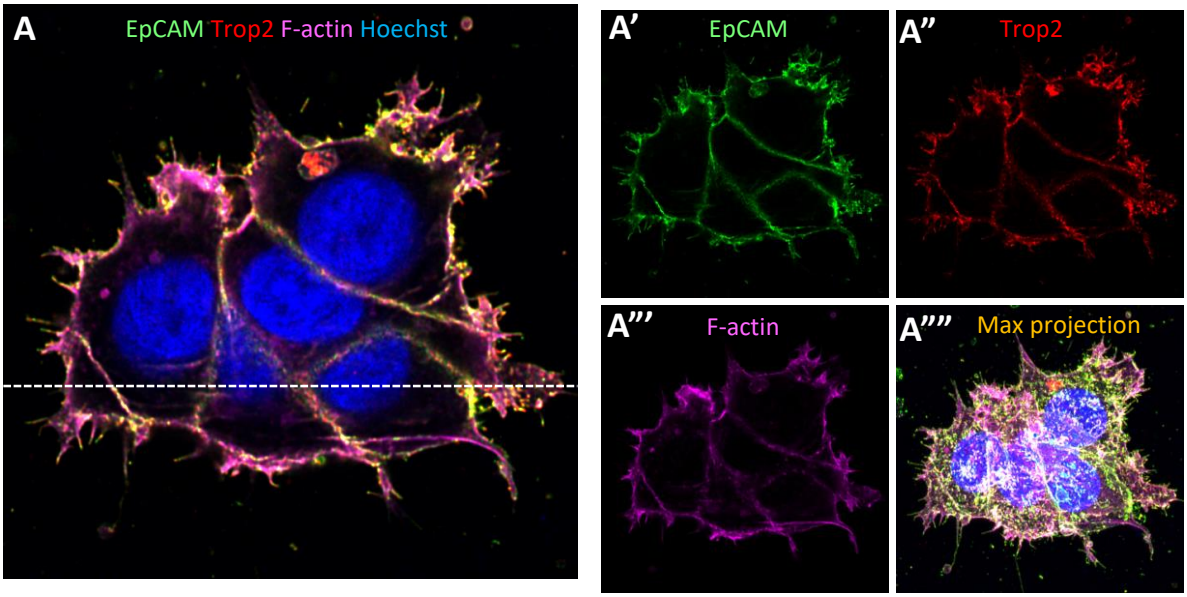
A
EpCAM Trop2 F-actin Hoechst
A'
EpCAM
A''
Trop2
A'''
F-actin
A''''
Max projection

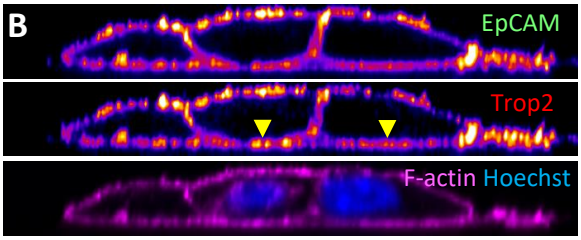
B
EpCAM
Trop2
F-actin Hoechst

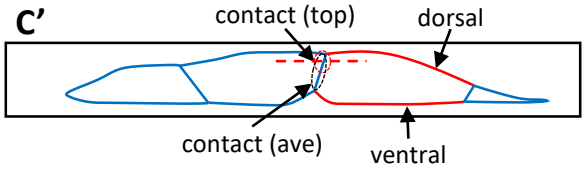
C'
contact (top)
dorsal
contact (ave)
ventral

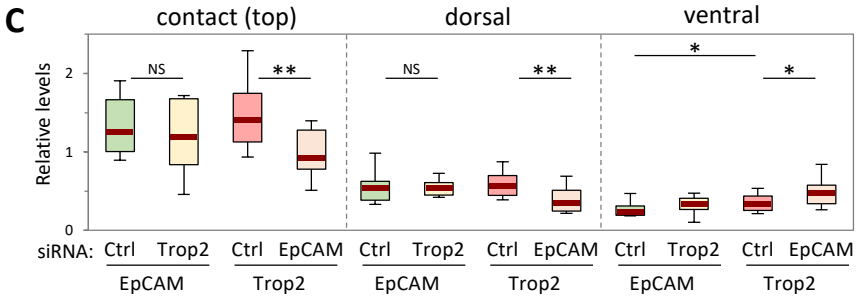
C
contact (top)
dorsal
ventral
Relative levels
NS
**
NS
**
*
*
siRNA: Ctrl Trop2 Ctrl EpCAM Ctrl Trop2 Ctrl EpCAM Ctrl Trop2 Ctrl EpCAM
EpCAM Trop2 EpCAM Trop2 EpCAM Trop2

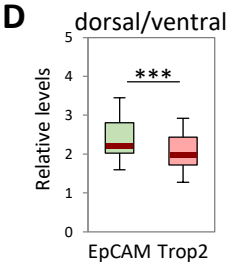
D
dorsal/ventral
Relative levels
***
EpCAM Trop2

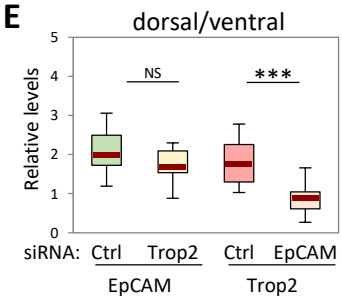
E
dorsal/ventral
Relative levels
NS
***
siRNA: Ctrl Trop2 Ctrl EpCAM
EpCAM Trop2

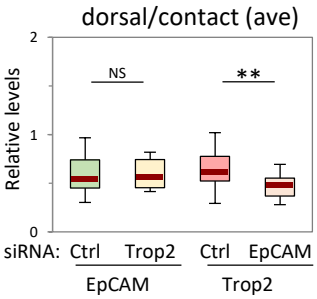
F
dorsal/contact (ave)
Relative levels
NS
**
siRNA: Ctrl Trop2 Ctrl EpCAM
EpCAM Trop2

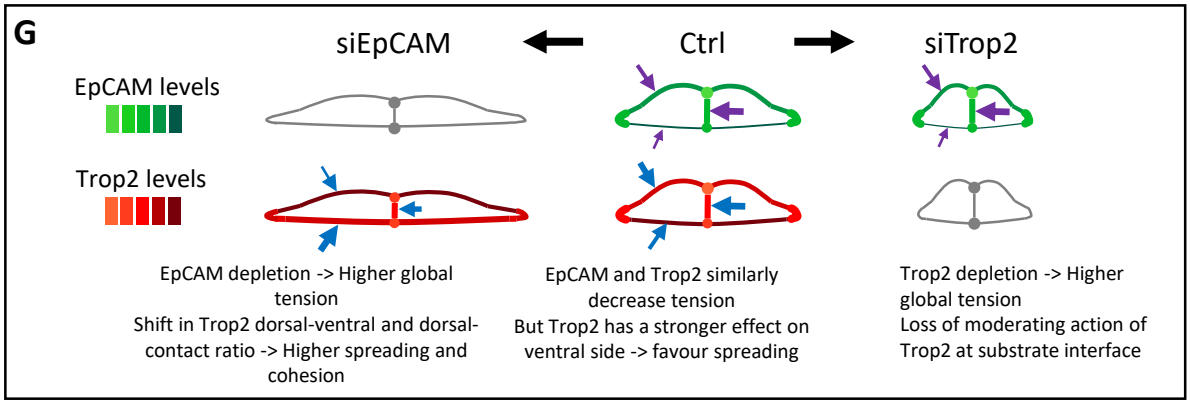
G
siEpCAM
Ctrl
siTrop2
EpCAM levels
Trop2 levels
EpCAM depletion -> Higher global tension
Shift in Trop2 dorsal-ventral and dorsal-contact ratio -> Higher spreading and cohesion
EpCAM and Trop2 similarly decrease tension
But Trop2 has a stronger effect on ventral side -> favour spreading
Trop2 depletion -> Higher global tension
Loss of moderating action of Trop2 at substrate interface

Figure 7

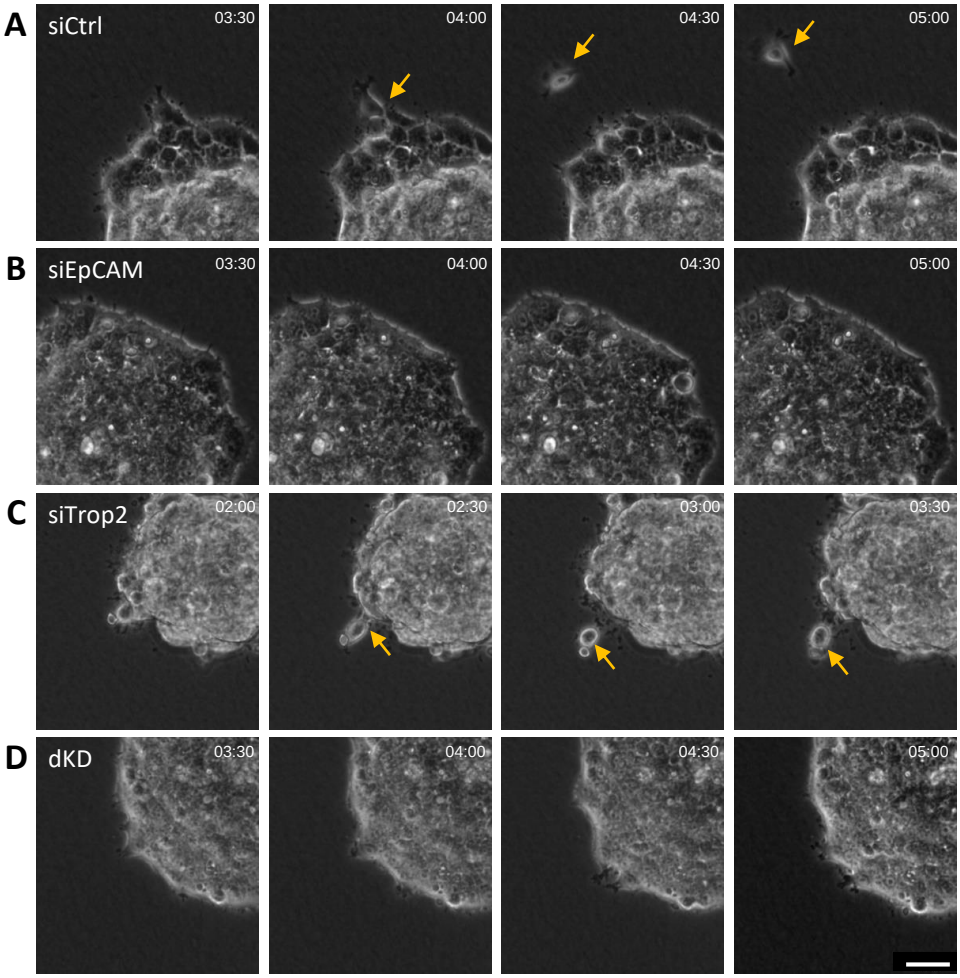
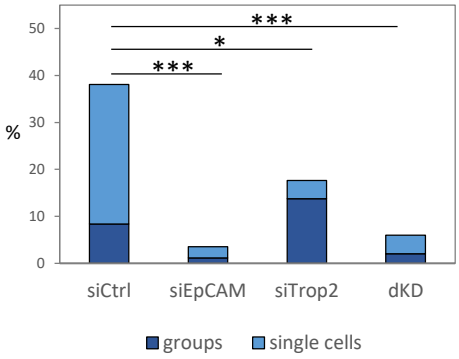
E Frequency of cell detachment and migration